MIT OpenCourseWare
http://ocw.mit.edu

Haus, Hermann A., and James R. Melcher. *Electromagnetic Fields and Energy.*
Englewood Cliffs, NJ: Prentice-Hall, 1989. ISBN: 9780132490207.

Please use the following citation format:

> Haus, Hermann A., and James R. Melcher, *Electromagnetic Fields and Energy*. (Massachusetts Institute of Technology: MIT OpenCourseWare). http://ocw.mit.edu (accessed [Date]). License: Creative Commons Attribution-NonCommercial-Share Alike.
>
> Also available from Prentice-Hall: Englewood Cliffs, NJ, 1989. ISBN: 9780132490207.

Note: Please use the actual date you accessed this material in your citation.

For more information about citing these materials or our Terms of Use, visit:
http://ocw.mit.edu/terms

13

ELECTRODYNAMIC FIELDS: THE BOUNDARY VALUE POINT OF VIEW

13.0 INTRODUCTION

In the treatment of EQS and MQS systems, we started in Chaps. 4 and 8, respectively, by analyzing the fields produced by specified (known) sources. Then we recognized that in the presence of materials, at least some of these sources were induced by the fields themselves. Induced surface charge and surface current densities were determined by making the fields satisfy boundary conditions. In the volume of a given region, fields were composed of particular solutions to the governing quasistatic equations (the scalar and vector Poisson equations for EQS and MQS systems, respectively) and those solutions to the homogeneous equations (the scalar and vector Laplace equation, respectively) that made the total fields satisfy appropriate boundary conditions.

We now embark on a similar approach in the analysis of electrodynamic fields. Chapter 12 presented a study of the fields produced by specified sources (dipoles, line sources, and surface sources) and obeying the inhomogeneous wave equation. Just as in the case of EQS and MQS systems in Chap. 5 and the last half of Chap. 8, we shall now concentrate on solutions to the homogeneous source-free equations. These solutions then serve to obtain the fields produced by sources lying outside (maybe on the boundary) of the region within which the fields are to be found. In the region of interest, the fields generally satisfy the inhomogeneous wave equation. However in this chapter, where there are no sources in the volume of interest, they satisfy the homogeneous wave equation. It should come as no surprise that, following this systematic approach, we shall reencounter some of the previously obtained solutions.

In this chapter, fields will be determined in some limited region such as the volume V of Fig. 13.0.1. The boundaries might be in part perfectly conducting in the sense that on their surfaces, $\mathbf{E}$ is perpendicular and the time-varying $\mathbf{H}$ is tangential. The surface current and charge densities implied by these conditions
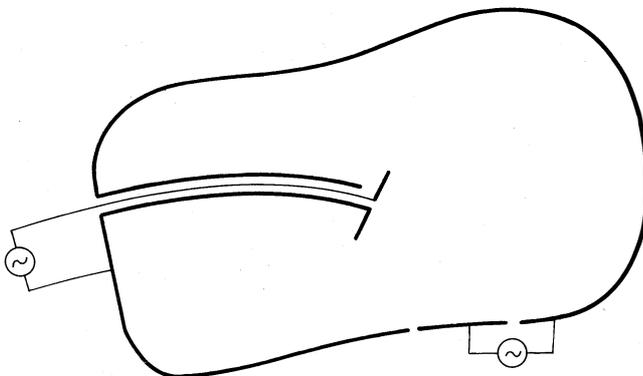
1

Fig. 13.0.1   Fields in a limited region are in part due to sources induced on boundaries by the fields themselves.

are not known until after the fields have been found. If there is material within the region of interest, it is perfectly insulating and of piece-wise uniform permittivity ϵ and permeability μ.[1] Sources $\mathbf{J}$ and ρ are specified throughout the volume and appear as driving terms in the inhomogeneous wave equations, (12.6.8) and (12.6.32). Thus, the $\mathbf{H}$ and $\mathbf{E}$ fields obey the inhomogeneous wave-equations.

$$\nabla^2\mathbf{H} - \mu\epsilon\frac{\partial^2\mathbf{H}}{\partial t^2} = -\nabla \times \mathbf{J} \tag{1}$$

$$\nabla^2\mathbf{E} - \mu\epsilon\frac{\partial^2\mathbf{E}}{\partial t^2} = \nabla\Big(\frac{\rho}{\epsilon}\Big) + \mu\frac{\partial\mathbf{J}}{\partial t} \tag{2}$$

As in earlier chapters, we might think of the solution to these equations as the sum of a part satisfying the inhomogeneous equations throughout V (particular solution), and a part satisfying the homogeneous wave equation throughout that region. In principle, the particular solution could be obtained using the superposition integral approach taken in Chap. 12. For example, if an electric dipole were introduced into a region containing a uniform medium, the particular solution would be that given in Sec. 12.2 for an electric dipole. The boundary conditions are generally not met by these fields. They are then satisfied by adding an appropriate solution of the homogeneous wave equation.[2]

In this chapter, the source terms on the right in (1) and (2) will be set equal to zero, and so we shall be concentrating on solutions to the homogeneous wave equation. By combining the solutions of the homogeneous wave equation that satisfy boundary conditions with the source-driven fields of the preceding chapter, one can describe situations with given sources and given boundaries.

In this chapter, we shall consider the propagation of waves in some axial direction along a structure that is uniform in that direction. Such waves are used to transport energy along pairs of conductors (transmission lines), and through

---

[1] If the region is one of free space, $\epsilon \to \epsilon_o$ and $\mu \to \mu_o$.

[2] As pointed out in Sec. 12.7, this is essentially what is being done in satisfying boundary conditions by the method of images.

waveguides (metal tubes at microwave frequencies and dielectric fibers at optical frequencies). We confine ourselves to the sinusoidal steady state.

Sections 13.1-13.3 study two-dimensional modes between plane parallel conductors. This example introduces the mode expansion of electrodynamic fields that is analogous to the expansion of the EQS field of the capacitive attenuator (in Sec. 5.5) in terms of the solutions to Laplace's equation. The principal and higher order modes form a complete set for the representation of arbitrary boundary conditions. The example is a model for a strip transmission line and hence serves as an introduction to the subject of Chap. 14. The higher-order modes manifest properties much like those found in Sec. 13.4 for hollow pipe guides.

The dielectric waveguides considered in Sec. 13.5 explain the guiding properties of optical fibers that are of great practical interest. Waves are guided by a dielectric core having permittivity larger than that of the surrounding medium but possess fields extending outside this core. Such electromagnetic waves are guided because the dielectric core slows the effective velocity of the wave in the guide to the point where it can match the velocity of a wave in the surrounding region that propagates along the guide but decays in a direction perpendicular to the guide.

The fields considered in Secs. 13.1–13.3 offer the opportunity to reinforce the notions of quasistatics. Connections between the EQS and MQS fields studied in Chaps. 5 and 8, respectively, and their corresponding electrodynamic fields are made throughout Secs. 13.1–13.4.

13.1 INTRODUCTION TO TEM WAVES

The **E** and **H** fields of transverse electromagnetic waves are directed transverse to the direction of propagation. It will be shown in Sec. 14.2 that such TEM waves propagate along structures composed of pairs of perfect conductors of arbitrary cross-section. The parallel plates shown in Fig. 13.1.1 are a special case of such a pair of conductors. The direction of propagation is along the y axis. With a source driving the conductors at the left, the conductors can be used to deliver electrical energy to a load connected between the right edges of the plates. They then function as a *parallel plate transmission line.*

We assume that the plates are wide in the z direction compared to the spacing, a, and that conditions imposed in the planes $y = 0$ and $y = -b$ are independent of z, so that the fields are also z independent. In this section, discussion is limited to either "open" electrodes at $y = 0$ or "shorted" electrodes. Techniques for dealing with arbitrarily terminated transmission lines will be introduced in Chap. 14. The "open" or "shorted" terminals result in standing waves that serve to illustrate the relationship between simple electrodynamic fields and the EQS and MQS limits. These fields will be generalized in the next two sections, where we find that the TEM wave is but one of an infinite number of modes of propagation along the y axis between the plates.

If the plates are open circuited at the right, as shown in Fig. 13.1.1, a voltage is applied at the left at $y = -b$, and the fields are EQS, the **E** that results is x directed. (The plates form a parallel plate capacitor.) If they are "shorted" at the right and the fields are MQS, the **H** that results from applying a current source at the left is z directed. (The plates form a one-turn inductor.) We are now looking
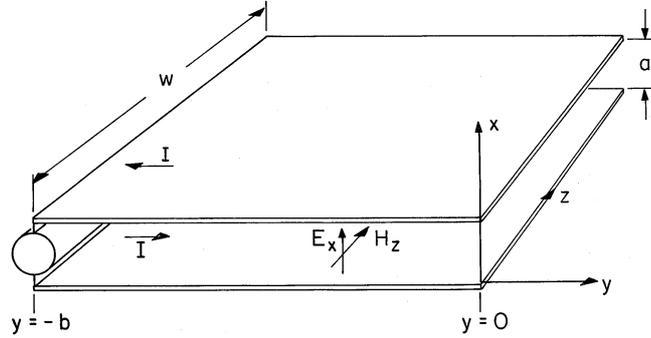
Fig. 13.1.1   Plane parallel plate transmission line.

for solutions to Maxwell's equations (12.0.7)–(12.0.10) that are similarly transverse to the y axis.

$$\mathbf{E} = E_x \mathbf{i_x}; \qquad \mathbf{H} = H_z \mathbf{i_z} \tag{1}$$

Fields of this form automatically satisfy the boundary conditions of zero tangential $\mathbf{E}$ and normal $\mathbf{H}$ (normal $\mathbf{B}$) on the surfaces of the perfect conductors. These fields have no divergence, so the divergence laws for $\mathbf{E}$ and $\mathbf{H}$ [(12.0.7) and (12.0.10)] are automatically satisfied. Thus, the remaining laws, Ampère's law (12.0.8) and Faraday's law (12.0.9) fully describe these TEM fields. We pick out the only components of these laws that are not automatically satisfied by observing that $\partial E_x / \partial t$ drives the x component of Ampère's law and $\partial H_z / \partial t$ is the source term of the z component of Faraday's law.

$$\boxed{\frac{\partial H_z}{\partial y} = \epsilon \frac{\partial E_x}{\partial t}} \tag{2}$$

$$\boxed{\frac{\partial E_x}{\partial y} = \mu \frac{\partial H_z}{\partial t}} \tag{3}$$

The other components of these laws are automatically satisfied if it is assumed that the fields are independent of the transverse coordinates and thus depend only on y.

The effect of the plates is to terminate the field lines so that there are no fields in the regions outside. With Gauss' continuity condition applied to the respective plates, E_x terminates on surface charge densities of opposite sign on the respective electrodes.

$$\sigma_s(x = 0) = \epsilon E_x; \qquad \sigma_s(x = a) = -\epsilon E_x \tag{4}$$

These relationships are illustrated in Fig. 13.1.2a.

The magnetic field is terminated on the plates by surface current densities. With Ampère's continuity condition applied to each of the plates,

$$K_y(x = 0) = -H_z; \qquad K_y(x = a) = H_z \tag{5}$$

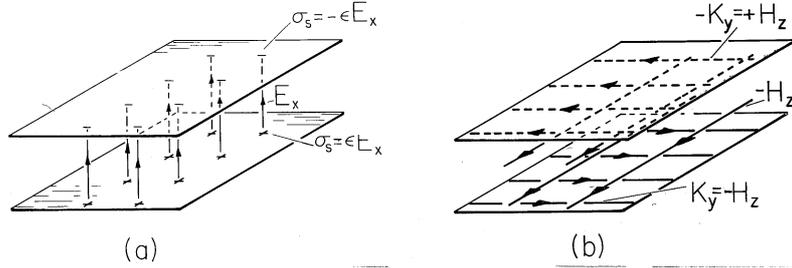**Fig. 13.1.2**   (a) Surface charge densities terminating **E** of TEM field between electrodes of Fig. 13.1.1. (b) Surface current densities terminating **H**.

these relationships are represented in Fig. 13.1.2b.

We shall be interested primarily in the sinusoidal steady state. Between the plates, the fields are governed by differential equations having constant coefficients. We therefore assume that the field response takes the form

$$H_z = \operatorname{Re} \hat{H}_z(y)e^{j\omega t}; \qquad E_x = \operatorname{Re} \hat{E}_x(y)e^{j\omega t} \tag{6}$$

where ω can be regarded as determined by the source that drives the system at one of the boundaries. Substitution of these solutions into (2) and (3) results in a pair of ordinary constant coefficient differential equations describing the y dependence of E_x and H_z. Without bothering to write these equations out, we know that they too will be satisfied by exponential functions of y. Thus, we proceed to look for solutions where the functions of y in (6) take the form $\exp(-jk_y y)$.

$$H_z = \operatorname{Re} \hat{h}_z e^{j(\omega t - k_y y)}; \qquad E_x = \operatorname{Re} \hat{e}_x e^{j(\omega t - k_y y)} \tag{7}$$

Once again, we have assumed a solution taking a product form. Substitution into (2) then shows that

$$\hat{e}_x = -\frac{k_y}{\omega\epsilon}\hat{h}_z \tag{8}$$

and substitution of this expression into (3) gives the *dispersion equation*

$$k_y = \pm\beta; \qquad \beta \equiv \omega\sqrt{\mu\epsilon} = \frac{\omega}{c} \tag{9}$$

For a given frequency, there are two values of k_y. A linear combination of the solutions in the form of (7) is therefore

$$H_z = \operatorname{Re}[A^+ e^{-j\beta y} + A^- e^{j\beta y}]e^{j\omega t} \tag{10}$$

The associated electric field follows from (8) evaluated for the $\pm$ waves, respectively, using $k_y = \pm\beta$.

$$E_x = -\operatorname{Re}\sqrt{\mu/\epsilon}[A^+ e^{-j\beta y} - A^- e^{j\beta y}]e^{j\omega t} \tag{11}$$

The amplitudes of the waves, A^+ and A^-, are determined by the boundary conditions imposed in planes perpendicular to the y axis. The following example
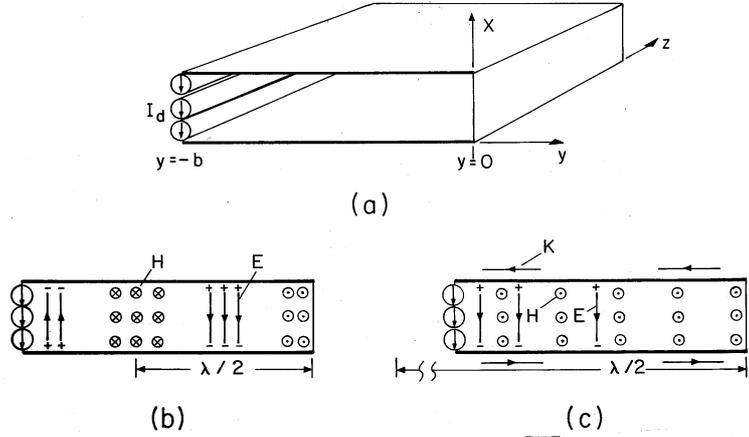
Fig. 13.1.3   (a) Shorted transmission line driven by a distributed current source. (b) Standing wave fields with **E** and **H** shown at times differing by 90 degrees. (c) MQS fields in limit where wavelength is long compared to length of system.

illustrates how the imposition of these *longitudinal boundary conditions* determines the fields. It also is the first of several opportunities we now use to place the EQS and MQS approximations in perspective.

Example 13.1.1.   Standing Waves on a Shorted Parallel Plate Transmission Line

In Fig. 13.1.3a, the parallel plates are terminated at $y = 0$ by a perfectly conducting plate. They are driven at $y = -b$ by a current source I_d distributed over the width w. Thus, there is a surface current density $K_y = I_d/w \equiv K_o$ imposed on the lower plate at $y = -b$. Further, in this example we will assume that a distribution of sources is used in the plane $y = -b$ to make this driving surface current density uniform over that plane. In summary, the longitudinal boundary conditions are

$$E_x(0, t) = 0 \tag{12}$$

$$H_z(-b, t) = -\text{Re}\,\hat{K}_o e^{j\omega t} \tag{13}$$

To make E_x as given by (11) satisfy the first of these boundary conditions, we must have the amplitudes of the two traveling waves equal.

$$A^+ = A^- \tag{14}$$

With this relation used to eliminate A^+ in (10), it follows from (13) that

$$A^+ = -\frac{\hat{K}_o}{2\cos\beta b} \tag{15}$$

We have found that the fields between the plates take the form of standing waves.

$$H_z = -\text{Re}\,\hat{K}_o \frac{\cos\beta y}{\cos\beta b} e^{j\omega t} \tag{16}$$

$$E_x = -\mathrm{Re}\, j \hat{K}_o \sqrt{\mu/\epsilon}\frac{\sin \beta y}{\cos \beta b}e^{j\omega t} \tag{17}$$

Note that $\mathbf{E}$ and $\mathbf{H}$ are $90°$ out of temporal phase.[3] When one is at its peak, the other is zero. The distributions of $\mathbf{E}$ and $\mathbf{H}$ shown in Fig. 13.1.3b are therefore at different instants in time.

Every half-wavelength π/β from the short, $\mathbf{E}$ is again zero, as sketched in Fig. 13.1.3b. Beginning at a distance of a quarter-wavelength from the short, the magnetic field also exhibits nulls at half-wavelength intervals. Adjacent peaks in a given field are 180 degrees out of temporal phase.

The MQS Limit.   If the driving frequency is so low that a wavelength is much longer than the length b, we have

$$\frac{2\pi b}{\lambda} = \beta b \ll 1 \tag{18}$$

In this limit, the fields are those of a one-turn inductor. That is, with $\sin(\beta y) \approx \beta y$ and $\cos(\beta y) \approx 1$, (16) and (17) become

$$H_z \to -\mathrm{Re}\, \hat{K}_o e^{j\omega t} \tag{19}$$

$$E_x \to -\mathrm{Re}\, \hat{K}_o j\omega \mu y e^{j\omega t} \tag{20}$$

The magnetic field intensity is uniform throughout and the surface current density circulates uniformly around the one-turn loop. The electric field increases in a linear fashion from zero at the short to a maximum at the source, where the source voltage is

$$v(t) = \int_0^a E_x(-b,t)dx = \mathrm{Re}\, \hat{K}_o j\omega \mu b a e^{j\omega t} = \frac{d\lambda}{dt} \tag{21}$$

To make it clear that these are the fields of a one-turn solenoid (Example 8.4.4), the flux linkage λ has been identified as

$$\lambda = L\frac{di}{dt}; \qquad i = \mathrm{Re}\, \hat{K}_o w e^{j\omega t}; \qquad L = \frac{ab\mu}{w} \tag{22}$$

where L is the inductance.

The MQS Approximation.   In Chap. 8, we would have been led to these same limiting fields by assuming at the outset that the displacement current, the term on the right in (2), is negligible. Then, this one-dimensional form of Ampère's law and (1) requires that

$$\nabla \times \mathbf{H} \approx 0 \Rightarrow \frac{\partial H_z}{\partial y} \approx 0 \Rightarrow H_z = H_z(t) = -\mathrm{Re}\, \hat{K}_o e^{j\omega t} \tag{23}$$

If we now use this finding in Faraday's law, (3), integration on y and use of the boundary condition of (12) gives the same result for $\mathbf{E}$ as found taking the low-frequency limit, (20).

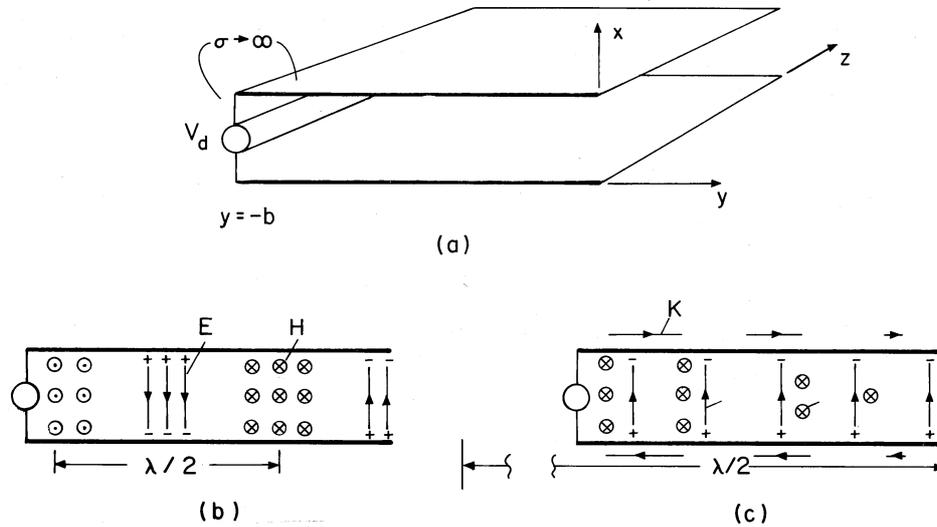[3] In making this and the following deductions, it is helpful to take $\hat{K}_o$ as being real.

Fig. 13.1.4   (a) Open circuit transmission line driven by voltage source. (b) **E** and **H** at times that differ by 90 degrees. (c) EQS fields in limit where wavelength is long compared to b.

In the previous example, the longitudinal boundary conditions (conditions imposed at planes of constant y) could be satisfied exactly using the TEM mode alone. The short at the right and the distributed current source at the left each imposed a condition that was, like the TEM fields, independent of the transverse coordinates. In almost all practical situations, longitudinal boundary conditions which are independent of the transverse coordinates (used to describe transmission lines) are approximate. The open circuit termination at $y = 0$, shown in Fig. 13.1.4, is a case in point, as is the source which in this case is not distributed in the x direction.

If a longitudinal boundary condition is independent of z, the fields are, in principle, still two dimensional. Between the plates, we can therefore think of satisfying the longitudinal boundary conditions using a superposition of the modes to be developed in the next section. These consist of not only the TEM mode considered here, but of modes having an x dependence. A detailed evaluation of the coefficients specifying the amplitudes of the higher-order modes brought in by the transverse dependence of a longitudinal boundary condition is illustrated in Sec. 13.3. There we shall find that at low frequencies, where these higher-order modes are governed by Laplace's equation, they contribute to the fields only in the vicinity of the longitudinal boundaries. As the frequency is raised beyond their respective cutoff frequencies, the higher-order modes begin to propagate along the y axis and so have an influence far from the longitudinal boundaries.

Here, where we wish to restrict ourselves to situations that are well described by the TEM modes, we restrict the frequency range of interest to well below the lowest cutoff frequency of the lowest of the higher-order modes.

Given this condition, "end effects" are restricted to the neighborhood of a longitudinal boundary. Approximate boundary conditions then determine the distribution of the TEM fields, which dominate over most of the length. In the open
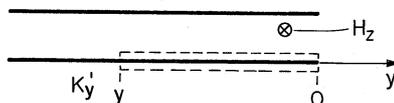
Fig. 13.1.5   The surface current density, and hence, H_z go to zero in the vicinity of the open end.

circuit example of Fig. 13.1.4a, application of the integral charge conservation law to a volume enclosing the end of one of the plates, as illustrated in Fig. 13.1.5, shows that K_y must be essentially zero at $y = 0$. For the TEM fields, this implies the boundary condition[4]

$$H_z(0, t) = 0 \tag{24}$$

At the left end, the vertical segments of perfect conductor joining the voltage source to the parallel plates require that E_x be zero over these segments. We shall show later that the higher-order modes do not contribute to the line integral of **E** between the plates. Thus, in so far as the TEM fields are concerned, the requirement is that

$$V_d(t) = \int_0^a E_x(-b, t)dx \Rightarrow E_x(-b, t) = \frac{V_d}{a} \tag{25}$$

Example 13.1.2.   Standing Waves on an Open-Circuit Parallel Plate
                     Transmission Line

Consider the parallel plates "open" at $y = 0$ and driven by a voltage source at $y = -b$. Boundary conditions are then

$$H_z(0, t) = 0; \qquad E_x(-b, t) = \operatorname{Re} \hat{V}_d e^{j\omega t}/a \tag{26}$$

Evaluation of the coefficients in (10) and (11) so that the boundary conditions in (26) are satisfied gives

$$A^+ = -A^- = -\frac{\hat{V}_d}{2a \cos \beta b} \sqrt{\epsilon/\mu} \tag{27}$$

It follows that the TEM fields between the plates, (10) and (11), are

$$H_z = \operatorname{Re} j \frac{\hat{V}_d}{a} \sqrt{\epsilon/\mu} \frac{\sin \beta y}{\cos \beta b} e^{j\omega t} \tag{28}$$

$$E_x = \operatorname{Re} \frac{\hat{V}_d}{a} \frac{\cos \beta y}{\cos \beta b} e^{j\omega t} \tag{29}$$

These distributions of **H** and **E** are shown in Fig. 13.1.4 at times that differ by 90 degrees. The standing wave is similar to that described in the previous example, except that it is now **E** rather than **H** that peaks at the open end.

---

[4] In the region outside, the fields are not confined by the plates. As a result, there is actually some radiation from the open end of the line, and this too is not represented by (24). This effect is small if the plate spacing is small compared to a wavelength.

The EQS Limit. In the low frequency limit, where the wavelength is much longer than the length of the plates so that $\beta b \ll 1$, the fields given by (28) and (29) become

$$H_z \to \mathrm{Re}\, j \frac{\hat{V}_d}{a} \omega \epsilon y e^{j\omega t} \tag{30}$$

$$E_x \to \mathrm{Re}\, \frac{\hat{V}_d}{a} e^{j\omega t} \tag{31}$$

At low frequencies, the fields are those of a capacitor. The electric field is uniform and simply equal to the applied voltage divided by the spacing. The magnetic field varies in a linear fashion from zero at the open end to its peak value at the voltage source. Evaluation of $-H_z$ at $z = -b$ gives the surface current density, and hence the current i, provided by the voltage source.

$$i = \mathrm{Re}\, j\omega \frac{\epsilon b w}{a} \hat{V}_d e^{j\omega t} \tag{32}$$

Note that this expression implies that

$$i = \frac{dq}{dt}; \qquad q = CV_d; \qquad C = \frac{\epsilon b w}{a} \tag{33}$$

so that the limiting behavior is indeed that of a plane parallel capacitor.

EQS Approximation. How would the quasistatic fields be predicted in terms of the TEM fields? If quasistatic, we expect the system to be EQS. Thus, the magnetic induction is negligible, so that the right-hand side of (3) is approximated as being equal to zero.

$$\nabla \times \mathbf{E} \approx 0 \Rightarrow \frac{\partial E_x}{\partial y} \approx 0 \tag{34}$$

It follows from integration of this expression and using the boundary condition of (26b) that the quasistatic $\mathbf{E}$ is

$$E_x = \frac{V_d}{a} \tag{35}$$

In turn, this result provides the displacement current density in Ampère's law, the right-hand side of (2).

$$\frac{\partial H_z}{\partial y} \simeq \epsilon \frac{d}{dt} \left(\frac{V_d}{a} \right) \tag{36}$$

The right-hand side of this expression is independent of y. Thus, integration with respect to y, with the "constant" of integration evaluated using the boundary condition of (26a), gives

$$H_z \simeq \epsilon \frac{d}{dt} V_d \frac{y}{a} \tag{37}$$

For the sinusoidal voltage drive assumed at the outset in the description of the TEM waves, this expression is consistent with that found in taking the quasistatic limit, (30).

Demonstration 13.1.1.   Visualization of Standing Waves

A demonstration of the fields described by the two previous examples is shown in Fig. 13.1.6. A pair of sheet metal electrodes are driven at the left by an oscillator. A fluorescent lamp placed between the electrodes is used to show the distribution of the rms electric field intensity.

The gas in the tube is ionized by the oscillating electric field. Through the field-induced acceleration of electrons in this gas, a sufficient velocity is reached so that collisions result in ionization and an associated optical radiation. What is seen is a time average response to an electric field that is oscillating far more rapidly than can be followed by the eye.

Because the light is proportional to the magnitude of the electric field, the observed 0.75 m distance between nulls is a half-wavelength. It can be inferred that the generator frequency is $f = c/\lambda = 3 \times 10^8/1.5 = 200$ MHz. Thus, the frequency is typical of the lower VHF television channels.

With the right end of the line shorted, the section of the lamp near that end gives evidence that the electric field there is indeed as would be expected from Fig. 13.1.3b, where it is zero at the short. Similarly, with the right end open, there is a peak in the light indicating that the electric field near that end is maximum. This is consistent with the picture given in Fig. 13.1.4b. In going from an open to a shorted condition, the positions of peak light intensity, and hence of peak electric field intensity, are shifted by $\lambda/4$.
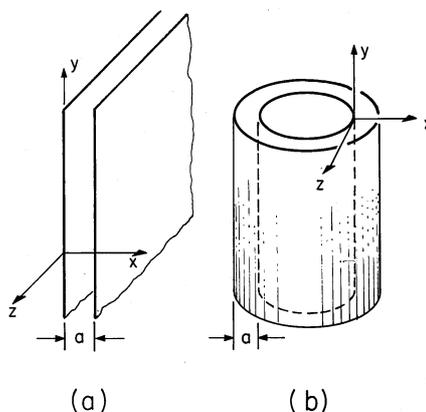
Fig. 13.2.1 (a) Plane parallel perfectly conducting plates. (b) Coaxial geometry in which z-independent fields of (a) might be approximately obtained without edge effects.

13.2 TWO-DIMENSIONAL MODES BETWEEN PARALLEL PLATES

This section treats the boundary value approach to finding the fields between the perfectly conducting parallel plates shown in Fig. 13.2.1a. Most of the mathematical ideas and physical insights that come from a study of modes on perfectly conducting structures that are uniform in one direction (for example, parallel wire and coaxial transmission lines and waveguides in the form of hollow perfectly conducting tubes) are illustrated by this example. In the previous section, we have already seen that the plates can be used as a transmission line supporting TEM waves. In this and the next section, we shall see that they are capable of supporting other electromagnetic waves.

Because the structure is uniform in the z direction, it can be excited in such a way that fields are independent of z. One way to make the structure approximately uniform in the z direction is illustrated in Fig. 13.2.1b, where the region between the plates becomes the annulus of coaxial conductors having very nearly the same radii. Thus, the difference of these radii becomes essentially the spacing a and the z coordinate maps into the ϕ coordinate. Another way is to make the plates very wide (in the z direction) compared to their spacing, a. Then, the fringing fields from the edges of the plates are negligible. In either case, the understanding is that the field excitation is uniformly distributed in the z direction. The fields are now assumed to be independent of z.

Because the fields are two dimensional, the classifications and relations given in Sec. 12.6 and summarized in Table 12.8.3 serve as our starting point. Cartesian coordinates are appropriate because the plates lie in coordinate planes. Fields either have **H** transverse to the $x - y$ plane and **E** in the $x - y$ plane (TM) or have **E** transverse and **H** in the $x - y$ plane (TE). In these cases, H_z and E_z are taken as the functions from which all other field components can be derived. We consider sinusoidal steady state solutions, so these fields take the form

$$H_z = \mathrm{Re}\ \hat{H}_z(x,y)e^{j\omega t} \tag{1}$$

$$E_z = \mathrm{Re}\ \hat{E}_z(x,y)e^{j\omega t} \tag{2}$$

These field components, respectively, satisfy the Helmholtz equation, (12.6.9) and (12.6.33) in Table 12.8.3, and the associated fields are given in terms of these components by the remaining relations in that table.

Once again, we find product solutions to the Helmholtz equation, where H_z and E_z are assumed to take the form $X(x)Y(y)$. This formalism for reducing a partial differential equation to ordinary differential equations was illustrated for Helmholtz's equation in Sec. 12.6. This time, we take a more mature approach, based on the observation that the coefficients of the governing equation are independent of y (are constants). As a result, $Y(y)$ will turn out to be governed by a constant coefficient differential equation. This equation will have exponential solutions. Thus, with the understanding that k_y is a yet to be determined constant (that will turn out to have two values), we assume that the solutions take the specific product forms

$$\hat{H}_z = \hat{h}_z(x)e^{-jk_y y} \tag{3}$$

$$\hat{E}_z = \hat{e}_z(x)e^{-jk_y y} \tag{4}$$

Then, the field relations of Table 12.8.3 become

TM Fields:

$$\frac{d^2\hat{h}_z}{dx^2} + p^2\hat{h}_z = 0 \tag{5}$$

where $p^2 \equiv \omega^2\mu\epsilon - k_y^2$

$$\hat{e}_x = -\frac{k_y}{\omega\epsilon}\hat{h}_z \tag{6}$$

$$\hat{e}_y = -\frac{1}{j\omega\epsilon}\frac{d\hat{h}_z}{dx} \tag{7}$$

TE Fields:

$$\frac{d^2\hat{e}_z}{dx^2} + q^2\hat{e}_z = 0 \tag{8}$$

where $q^2 \equiv \omega^2\mu\epsilon - k_y^2$

$$\hat{h}_x = \frac{k_y}{\omega\mu}\hat{e}_z \tag{9}$$

$$\hat{h}_y = \frac{1}{j\omega\mu}\frac{d\hat{e}_z}{dx} \tag{10}$$

The boundary value problem now takes a classic form familiar from Sec. 5.5. What values of p and q will make the electric field tangential to the plates zero? For the TM fields, $\hat{e}_y = 0$ on the plates, and it follows from (7) that it is the derivative of H_z that must be zero on the plates. For the TE fields, E_z must itself be zero at the plates. Thus, the boundary conditions are

TM Fields:

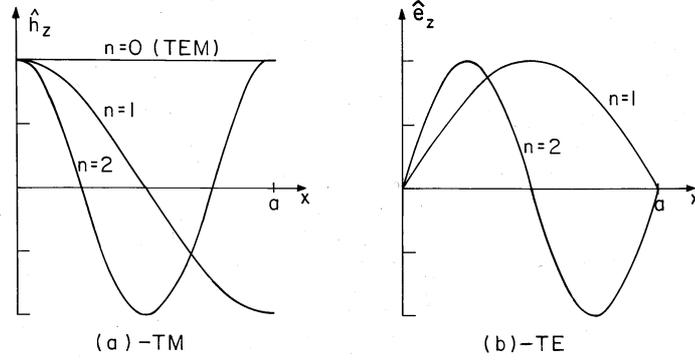$$\frac{d\hat{h}_z}{dx}(0) = 0; \qquad \frac{d\hat{h}_z}{dx}(a) = 0 \tag{11}$$

Fig. 13.2.2   Dependence of fundamental fields on x.

TE Fields:

$$\hat{e}_z(0) = 0; \qquad \hat{e}_z(a) = 0 \tag{12}$$

To check that all of the conditions are indeed met at the boundaries, note that if (11) is satisfied, there is neither a tangential **E** nor a normal **H** at the boundaries for the TM fields. (There is no normal **H** whether the boundary condition is satisfied or not.) For the TE field, E_z is the only electric field, and making $E_z=0$ on the boundaries indeed guarantees that $H_x = 0$ there, as can be seen from (9).

Representing the TM modes, the solution to (5) is a linear combination of $\sin(px)$ and $\cos(px)$. To satisfy the boundary condition, (11), at $x = 0$, we must select $\cos(px)$. Then, to satisfy the condition at $x = a$, it follows that $p = p_n = n\pi/a$, $n = 0, 1, 2, \ldots$

$$\hat{h}_z \propto \cos p_n x \tag{13}$$

$$p_n = \frac{n\pi}{a}, \quad n = 0, 1, 2, \ldots \tag{14}$$

These functions and the associated values of p are called *eigenfunctions* and *eigenvalues*, respectively. The solutions that have been found have the x dependence shown in Fig. 13.2.2a.

From the definition of p given in (5), it follows that for a given frequency ω (presumably imposed by an excitation), the wave number k_y associated with the n-th mode is

$$k_y \equiv \pm\beta_n; \qquad \beta_n \equiv \begin{cases} \sqrt{\omega^2\mu\epsilon - (n\pi/a)^2}; & \omega^2\mu\epsilon > (n\pi/a)^2 \\ -j\sqrt{(n\pi/a)^2 - \omega^2\mu\epsilon}; & \omega^2\mu\epsilon < (n\pi/a)^2 \end{cases} \tag{15}$$

Similar reasoning identifies the modes for the TE fields. Of the two solutions to (8), the one that satisfies the boundary condition at $x = 0$ is $\sin(qx)$. The second boundary condition then requires that q take on certain eigenvalues, q_n.

$$\hat{e}_z \propto \sin q_n x \tag{16}$$

$$q_n = \frac{n\pi}{a} \tag{17}$$

The x dependence of E_z is then as shown in Fig. 13.2.2b. Note that the case $n = 0$ is excluded because it implies a solution of zero amplitude.

For the TE fields, it follows from (17) and the definition of q given with (8) that[5]

$$k_y \equiv \pm\beta_n; \qquad \beta_n \equiv \begin{cases} \sqrt{\omega^2\mu\epsilon - (n\pi/a)^2}; & \omega^2\mu\epsilon > (n\pi/a)^2 \\ -j\sqrt{(n\pi/a)^2 - \omega^2\mu\epsilon}; & \omega^2\mu\epsilon < (n\pi/a)^2 \end{cases} \qquad (18)$$

In general, the fields between the plates are a linear combination of all of the modes. In superimposing these modes, we recognize that $k_y = \pm\beta_n$. Thus, with coefficients that will be determined by boundary conditions in planes of constant y, we have the solutions

TM Modes:

$$\begin{aligned} H_z = &\mathrm{Re} \Big[A_o^+ e^{-j\beta_o y} + A_o^- e^{j\beta_o y} \\ &+ \sum_{n=1}^{\infty} \left(A_n^+ e^{-j\beta_n y} + A_n^- e^{j\beta_n y} \right) \cos\frac{n\pi}{a}x \Big] e^{j\omega t} \end{aligned} \qquad (19)$$

TE Modes:

$$E_z = \mathrm{Re} \sum_{n=1}^{\infty} \left(C_n^+ e^{-j\beta_n y} + C_n^- e^{j\beta_n y} \right) \sin\frac{n\pi}{a}x \, e^{j\omega t} \qquad (20)$$

We shall refer to the n-th mode represented by these fields as the TM_n or TE_n mode, respectively.

We now make an observation about the TM_0 mode that is of far-reaching significance. Its distribution of H_z has no dependence on x [(13) with $p_n = 0$]. As a result, $E_y = 0$ according to (7). Thus, for the TM_0 mode, *both* **E** and **H** are transverse to the axial direction y. This special mode, represented by the $n = 0$ terms in (19), is therefore the *transverse electromagnetic* (TEM) mode featured in the previous section. One of its most significant features is that the relation between frequency ω and wave number in the y direction, k_y, [(15) with $n = 0$] is $k_y = \pm\omega\sqrt{\mu\epsilon} = \pm\omega/c$, the same as for a uniform electromagnetic plane wave. Indeed, as we saw in Sec. 13.1, it *is* a uniform plane wave.

The frequency dependence of k_y for the TEM mode and for the higher-order TM_n modes given by (15) are represented graphically by the $\omega - k_y$ plot of Fig. 13.2.3. For a given frequency, ω, there are two values of k_y which we have called $\pm\beta_n$. The dashed curves represent imaginary values of k_y. Imaginary values correspond to exponentially decaying and "growing" solutions. An exponentially "growing" solution is in fact a solution that decays in the $-y$ direction. Note that the switch from exponentially decaying to propagating fields for the higher-order modes occurs at the *cutoff frequency*

$$\omega_{cn} = \frac{1}{\sqrt{\mu\epsilon}}\left(\frac{n\pi}{a}\right) \qquad (21)$$

---

[5] For the particular geometry considered here, it has turned out that the eigenvalues p_n and q_n are the same (with the exception of $n = 0$). This coincidence does not occur with boundaries having other geometries.
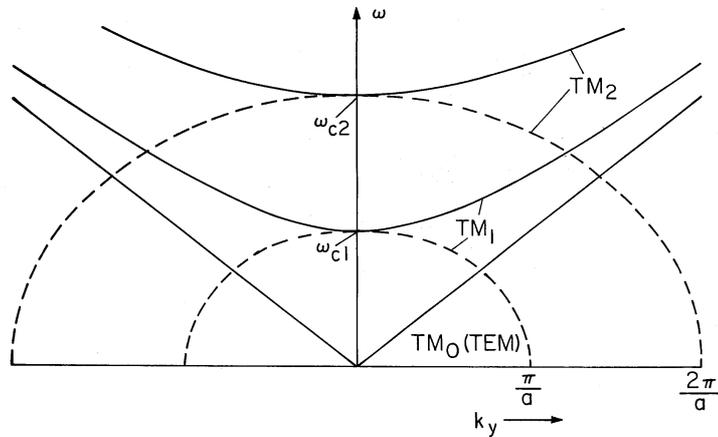
Fig. 13.2.3   Dispersion relation for TM modes.
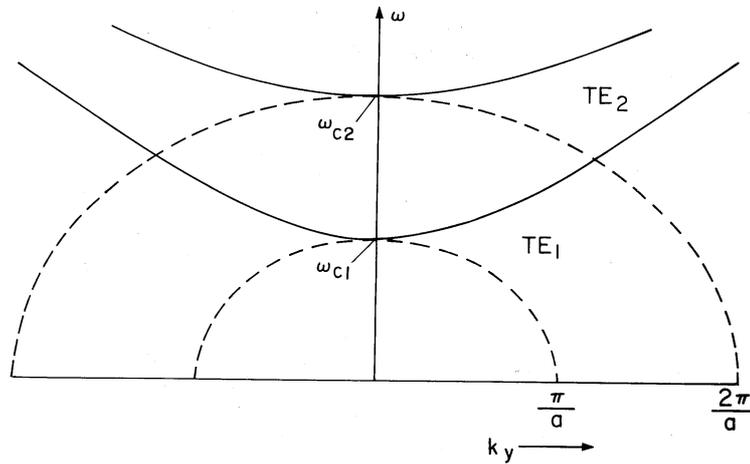

Fig. 13.2.4   Dispersion relation for TE modes.

The velocity of propagation of points of constant phase (for example, a point at which a field component is zero) is ω/k_y. Figure 13.2.3 emphasizes that for all but the TEM mode, the phase velocity is a function of frequency. The equation relating ω to k_y represented by this figure, (15), is often called the *dispersion equation*.

The dispersion equation for the TE modes is shown in Fig. 13.2.4. Although the field distributions implied by each branch are very different, in the case of the plane parallel electrodes considered here, the curves are the same as those for the $\mathrm{TM}_{n\neq0}$ modes.

The next section will provide greater insight into the higher-order TM and TE modes.

13.3 TE AND TM STANDING WAVES BETWEEN PARALLEL PLATES

In this section, we delve into the relationship between the two-dimensional higher-order modes derived in Sec. 13.2 and their sources. The examples are chosen to relate directly to case studies treated in quasistatic terms in Chaps. 5 and 8.

The matching of a longitudinal boundary condition by a superposition of modes may at first seem to be a purely mathematical process. However, even qualitatively it is helpful to *think* of the influence of an excitation in terms of the resulting modes. For quasistatic systems, this has already been our experience. For the purpose of estimating the dependence of the output signal on the spacing b between excitation and detection electrodes, the EQS response of the capacitive attenuator of Sec. 5.5 could be pictured in terms of the lowest-order mode. In the electrodynamic situations of interest here, it is even more common that one mode dominates. Above its cutoff frequency, a given mode can propagate through a waveguide to regions far removed from the excitation.

Modes obey orthogonality relations that are mathematically useful for the evaluation of the mode amplitudes. Formally, the mode orthogonality is implied by the differential equations governing the transverse dependence of the fundamental field components and the associated boundary conditions. For the TM modes, these are (13.2.5) and (13.2.11).

TM Modes:

$$\frac{d^2\hat{h}_{zn}}{dx^2} + p_n^2\hat{h}_{zn} = 0 \tag{1}$$

where

$$\frac{d\hat{h}_{zn}}{dx}(a) = 0; \qquad \frac{d\hat{h}_{zn}}{dx}(0) = 0$$

and for the TE modes, these are (13.2.8) and (13.2.12).

TE Modes:

$$\frac{d^2\hat{e}_{zn}}{dx^2} + q_n^2\hat{e}_{zn} = 0 \tag{2}$$

where

$$\hat{e}_{zn}(a) = 0; \qquad \hat{e}_{zn}(0) = 0$$

The word "orthogonal" is used here to mean that

$$\int_0^a \hat{h}_{zn}\hat{h}_{zm}dx = 0; \qquad n \neq m \tag{3}$$

$$\int_0^a \hat{e}_{zn}\hat{e}_{zm}dx = 0; \qquad n \neq m \tag{4}$$

These properties of the modes can be seen simply by carrying out the integrals, using the modes as given by (13.2.13) and (13.2.16). More fundamentally, they can be deduced from the differential equations and boundary conditions themselves, (1) and (2). This was illustrated in Sec. 5.5 using arguments that are directly applicable here [(5.5.20)–(5.5.26)].
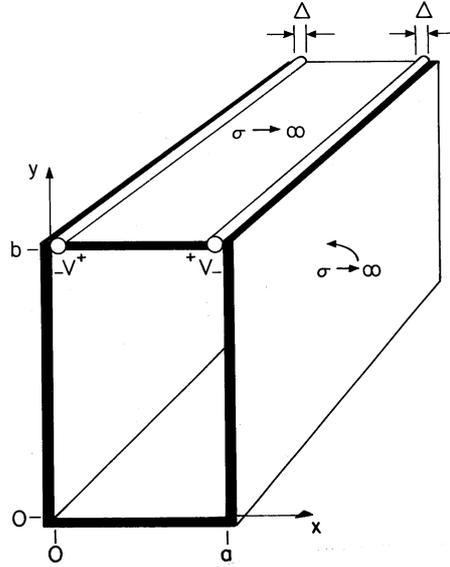
Fig. 13.3.1   Configuration for excitation of TM waves.

The following two examples illustrate how TE and TM modes can be excited in waveguides. In the quasistatic limit, the configurations respectively become identical to EQS and MQS situations treated in Chaps. 5 and 8.

Example 13.3.1.   Excitation of TM Modes and the EQS Limit

In the configuration shown in Fig. 13.3.1, the parallel plates lying in the planes $x = 0$ and $x = a$ are shorted at $y = 0$ by a perfectly conducting plate. The excitation is provided by distributed voltage sources driving a perfectly conducting plate in the plane $y = b$. These sources constrain the integral of **E** across narrow insulating gaps of length Δ between the respective edges of the upper plate and the adjacent plates. All the conductors are modeled as perfect. The distributed voltage sources maintain the two-dimensional character of the fields even as the width in the z direction becomes long compared to a wavelength. Note that the configuration is identical to that treated in Sec. 5.5. Therefore, we already know the field behavior in the quasistatic (low frequency) limit.

In general, the two-dimensional fields are the sum of the TM and TE fields. However, here the boundary conditions can be met by the TM fields alone. Thus, we begin with H_z, (13.2.19), expressed as a single sum.

$$H_z = \mathrm{Re} \Big[\sum_{n=0}^{\infty} (A_n^+ e^{-j\beta_n y} + A_n^- e^{j\beta_n y}) \cos \frac{n\pi}{a} x \Big] e^{j\omega t} \tag{5}$$

This field and the associated **E** satisfy the boundary conditions on the parallel plates at $x = 0$ and $x = a$. Boundary conditions are imposed on the tangential **E** at the longitudinal boundaries, where $y = 0$

$$E_x(x, 0, t) = 0 \tag{6}$$

and at the driving electrode, where $y = b$. We assume here that the gap lengths Δ are small compared to other dimensions of interest. Then, the electric field within each gap is conservative and the line integral of E_x across the gaps is equal to the gap voltages $\pm v$. Over the region between $x = \Delta$ and $x = a - \Delta$, the perfectly conducting electrode makes $E_x = 0$.

$$\int_{a-\Delta}^{a} E_x(x, b, t)dx = v; \qquad \int_{0}^{\Delta} E_x(x, b, t)dx = -v \tag{7}$$

Because the longitudinal boundary conditions are on E_x, we substitute H_z as given by (5) into the x component of Faraday's law [(12.6.6) of Table 12.8.3] to obtain

$$E_x = \text{Re} \Big[\sum_{n=0}^{\infty} \frac{-\beta_n}{\omega \epsilon} (A_n^+ e^{-j\beta_n y} - A_n^- e^{j\beta_n y}) \cos \frac{n\pi}{a} x \Big] e^{j\omega t} \tag{8}$$

To satisfy the condition at the short, (6), $A_n^+ = A_n^-$ and (8) becomes

$$E_x = \text{Re} \Big[\sum_{n=0}^{\infty} \frac{2j\beta_n}{\omega \epsilon} A_n^+ \sin \beta_n y \cos \frac{n\pi}{a} x \Big] e^{j\omega t} \tag{9}$$

This set of solutions satisfies the boundary conditions on three of the four boundaries. What we now do to satisfy the "last" boundary condition differs little from what was done in Sec. 5.5. The A_n^+'s are adjusted so that the summation of product solutions in (9) matches the boundary condition at $y = b$ summarized by (7). Thus, we write (9) with $y = b$ on the right and with the function representing (7) on the left. This expression is multiplied by the m'th eigenfunction, $\cos(m\pi x/a)$, and integrated from $x = 0$ to $x = a$.

$$\int_{0}^{a} \hat{E}_x(x, b) \cos \frac{m\pi x}{a} dx = \int_{0}^{a} \sum_{n=0}^{\infty} \frac{2j\beta_n A_n^+}{\omega \epsilon} \sin \beta_n b \cdot$$
$$\cos \frac{n\pi}{a} x \, \cos \frac{m\pi}{a} x dx \tag{10}$$

Because the intervals where $\hat{E}_x(x, b)$ is finite are so small, the cosine function can be approximated by a constant, namely ± 1 as appropriate. On the right-hand side of (10), we exploit the orthogonality condition so as to pick out only one term in the infinite series.

$$\hat{v}[-1 + \cos m\pi] = \frac{2j\beta_m}{\omega \epsilon} \sin \beta_m b \Big(\frac{a}{2} \Big) A_m^+ \tag{11}$$

Of the infinite number of terms in the integral on the right in (10), only the term where $n = m$ has contributed. The coefficients follow from solving (11) and replacing $m \to n$.

$$A_n^+ = \begin{cases} 0; & n \text{ even} \\ \dfrac{-2\omega \epsilon \hat{v}}{j\beta_n a \sin \beta_n b}; & n \text{ odd} \end{cases} \tag{12}$$

With the coefficients $A_n^+ = A_n^-$ now determined, we can evaluate all of the fields. Substitution into (5), and (8) and into the result using (12.6.7) from Table 12.8.3 gives

$$H_z = \mathrm{Re}\left[\sum_{\substack{n=1 \\ \text{odd}}}^{\infty} \frac{4j\omega\epsilon\hat{v}}{\beta_n a}\frac{\cos\beta_n y}{\sin\beta_n b}\cos\frac{n\pi}{a}x\right]e^{j\omega t} \tag{13}$$

$$E_x = \mathrm{Re}\left[\sum_{\substack{n=1 \\ \text{odd}}}^{\infty} \frac{-4\hat{v}}{a}\frac{\sin\beta_n y}{\sin\beta_n b}\cos\frac{n\pi}{a}x\right]e^{j\omega t} \tag{14}$$

$$E_y = \mathrm{Re}\left[\sum_{\substack{n=1 \\ \text{odd}}}^{\infty} \frac{4n\pi}{a}\frac{\hat{v}}{(\beta_n a)}\frac{\cos\beta_n y}{\sin\beta_n b}\sin\frac{n\pi}{a}x\right]e^{j\omega t} \tag{15}$$

Note the following aspects of these fields (which we can expect to see in Demonstration 13.3.1). First, the magnetic field is directed perpendicular to the $x-y$ plane. Second, by making the excitation symmetric, we have eliminated the TEM mode. As a result, the only modes are of order $n = 1$ and higher. Third, at frequencies below the cutoff for the TM$_1$ mode, β_y is imaginary and the fields decay in the y direction.[6] Indeed, in the quasistatic limit where $\omega^2\mu\epsilon \ll (\pi/a)^2$, the electric field is the same as that given by taking the gradient of (5.5.9). In this same quasistatic limit, the magnetic field would be obtained by using this quasistatic **E** to evaluate the displacement current and then solving for the resulting magnetic field subject to the boundary condition that there be no normal flux density on the surfaces of the perfect conductors. Fourth, above the cutoff frequency for the $n = 1$ mode but below the cutoff for the $n = 2$ mode, we should find standing waves having a wavelength $2\pi/\beta_1$.

Finally, note that each of the expressions for the field components has $\sin(\beta_n b)$ in its denominator. With the frequency adjusted such that $\beta_n = n\pi/b$, this function goes to zero and the fields become infinite. This resonance condition results in an infinite response, because we have pictured all of the conductors as perfect. It occurs when the frequency is adjusted so that a wave reflected from one boundary arrives at the other with just the right phase to reinforce, upon a second reflection, the wave currently being initiated by the drive.

The following experiment gives the opportunity to probe the fields that have been found in the previous example. In practical terms, the structure considered might be a parallel plate waveguide.

Demonstration 13.3.1.   Evanescent and Standing TM Waves

The experiment shown in Fig. 13.3.2 is designed so that the field distributions can be probed as the excitation is varied from below to above the cutoff frequency of the TM$_1$ mode. The excitation structures are designed to give fields approximating those found in Example 13.3.1. For convenience, $a = 4.8$ cm so that the excitation frequency ranges above and below a cut-off frequency of 3.1 GHz. The generator is modulated at an audible frequency so that the amplitude of the detected signal is converted to "loudness" of the tone from the loudspeaker.

In this TM case, the driving electrode is broken into segments, each insulated from the parallel plates forming the waveguide and each attached at its center to a

---

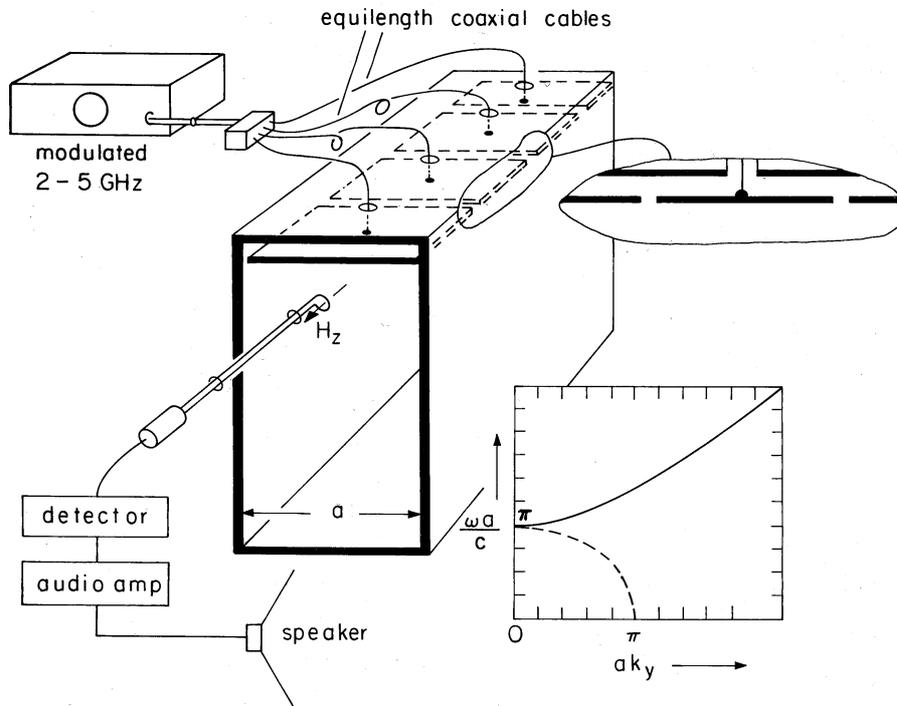[6] $\sin(ju) = j\sinh(u)$ and $\cos(ju) = \cosh(u)$

Fig. 13.3.2 Demonstration of TM evanescent and standing waves.

coaxial line from the generator. The segments insure that the fields applied to each part of the electrode are essentially in phase. (The cables feeding each segment are of the same length so that signals arrive at each segment in phase.) The width of the structure in the z direction is of the order of a wavelength or more to make the fields two dimensional. (Remember, in the vicinity of the lowest cutoff frequency, a is about one-half wavelength.) Thus, if the feeder were attached to a contiguous electrode at one point, there would be a tendency for standing waves to appear on the excitation electrode, much as they did on the wire antennae in Sec. 12.4. In the experiment, the segments are about a quarter-wavelength in the z direction but, of course, about a half-wavelength in the x direction.

In the experiment, **H** is detected by means of a one-turn coil. The voltage induced at the terminals of this loop is proportional to the magnetic flux perpendicular to the loop. Thus, for the TM fields, the loop detects its greatest signal when it is placed in an $x - y$ plane. To avoid interference with **E**, the coaxial line connected to the probe as well as the loop itself are kept adjacent to the conducting walls (where H_z peaks anyway).

The spatial features of the field, implied by the normalized ω versus k_y plot of Fig. 13.3.2, can be seen by moving the probe about. With the frequency below cutoff, the field decays in the $-y$ direction. This exponential decay or evanescence decreases to a linear dependence at cutoff and is replaced above cutoff by standing waves. The value of k_y at a given frequency can be deduced from the experiment by measuring the quarter-wave distance from the short to the first null in the magnetic field. Note that if there are asymmetries in the excitation that result in excitation of the TEM mode, the standing waves produced by this mode will tend to obscure

the TM$_1$ mode when it is evanescent. The TEM waves do not have a cutoff!

As we have seen once again, the TM fields are the electrodynamic generalization of two-dimensional EQS fields. That is, in the quasistatic limit, the previous example becomes the capacitive attenuator of Sec. 5.5.[7]

We have more than one reason to expect that the two-dimensional TE fields are the generalization of MQS systems. First, this was seen to be the case in Sec. 12.6, where the TE fields associated with a given surface current density were found to approach the MQS limit as $\omega^2 \mu\epsilon \ll k_y^2$. Second, from Sec. 8.6 we know that for every two-dimensional EQS configuration involving perfectly conducting boundaries, there is an MQS one as well.[8] In particular, the MQS analog of the capacitor attenuator is the configuration shown in Fig. 13.3.3. The MQS **H** field was found in Example 8.6.3.

In treating MQS fields in the presence of perfect conductors, we recognized that the condition of zero tangential **E** implied that there be no time-varying normal **B**. This made it possible to determine **H** without regard for **E**. We could then delay taking detailed account of **E** until Sec. 10.1. Thus, in the MQS limit, a system involving essentially a two-dimensional distribution of **H** can (and usually does) have an **E** that depends on the third dimension. For example, in the configuration of Fig. 13.3.3, a voltage source might be used to drive the current in the z direction through the upper electrode. This current is returned in the perfectly conducting ⊔-shaped walls. The electric fields in the vicinities of the gaps must therefore increase in the z direction from zero at the shorts to values consistent with the voltage sources at the near end. Over most of the length of the system, **E** is across the gap and therefore in planes *perpendicular* to the z axis. This MQS configuration does not excite pure TE fields. In order to produce (approximately) two-dimensional TE fields, provision must be made to make **E** as well as **H** two dimensional. The following example and demonstration give the opportunity to further develop an appreciation for TE fields.

Example 13.3.2.   Excitation of TE Modes and the MQS Limit

An idealized configuration for exciting standing TE modes is shown in Fig. 13.3.4. As in Example 13.3.1, the perfectly conducting plates are shorted in the plane $y = 0$. In the plane $y = b$ is a perfectly conducting plate that is segmented in the z direction. Each segment is driven by a voltage source that is itself distributed in the x direction. In the limit where there are many of these voltage sources and perfectly conducting segments, the driving electrode becomes one that both imposes a z-directed **E** and has no z component of **B**. That is, just below the surface of this electrode, wE_z is equal to the sum of the source voltages. One way of approximately realizing this idealization is used in the next demonstration.

Let Λ be defined as the flux per unit length (length taken along the z direction) into and out of the enclosed region through the gaps of width Δ between the driving electrode and the adjacent edges of the plane parallel electrodes. The magnetic field

---

[7] The example which was the theme of Sec. 5.5 might equally well have been called the "microwave attenuator," for a section of waveguide operated below cutoff is used in microwave circuits to attenuate signals.

[8] The **H** satisfying the condition that $\mathbf{n} \cdot \mathbf{B} = 0$ on the perfectly conducting boundaries was obtained by replacing $\Phi \to A_z$ in the solution to the analogous EQS problem.
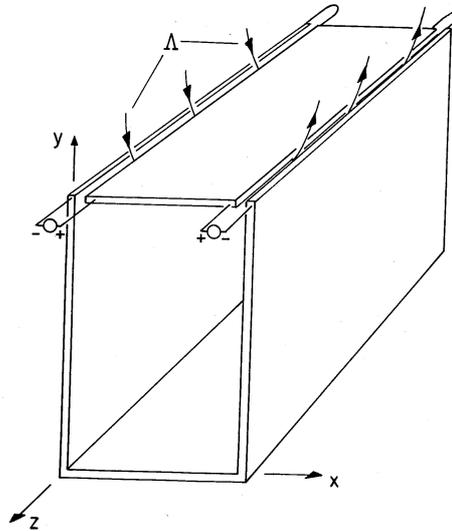
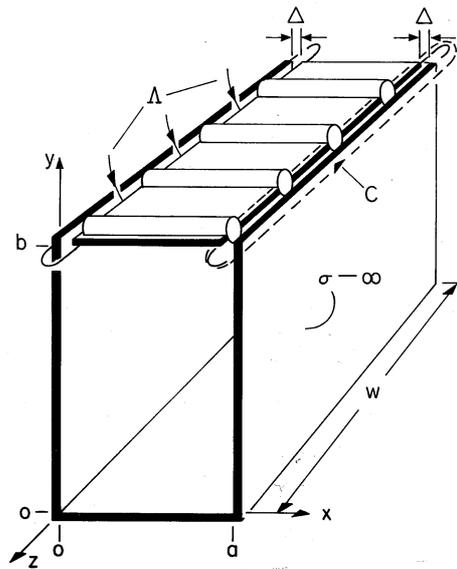**Fig. 13.3.3** Two-dimensional MQS configuration that does not have TE fields.

Fig. 13.3.4 Idealized configuration for excitation of TE standing waves.

normal to the driving electrode between the gaps is zero. Thus, at the upper surface, H_y has the distribution shown in Fig. 13.3.5a.

Faraday's integral law applied to the contour C of Fig. 13.3.4 and to a similar contour around the other gap shows that
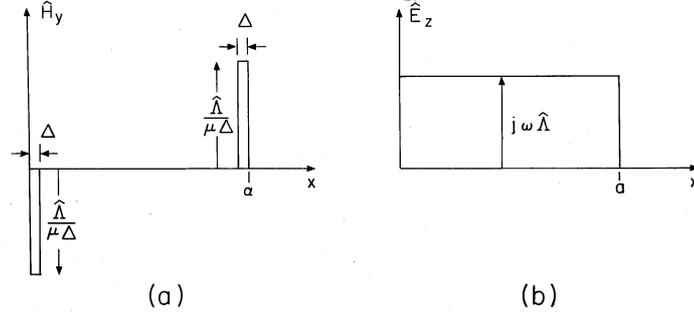
$$E_z(x,b,t) = -\frac{d\Lambda}{dt} \Rightarrow \hat{E}_z = -j\omega\hat{\Lambda} \tag{16}$$

Fig. 13.3.5 Equivalent boundary conditions on normal **H** and tangential **E** at $y = b$.

Thus, either the normal **B** or the tangential **E** on the surface at $y = b$ is specified. The two must be consistent with each other, i.e., they must obey Faraday's law. It is perhaps easiest in this case to deal directly with E_z in finding the coefficients appearing in (13.2.20). Once they have been determined (much as in Example 13.3.1), **H** follows from Faraday's law, (12.6.29) and (12.6.30) of Table 12.8.3.

$$E_z = \text{Re} \sum_{\substack{m=1 \\ \text{odd}}}^{\infty} -\frac{4j\hat{\Lambda}\omega}{m\pi} \frac{\sin\beta_m y}{\sin\beta_m b} \sin\frac{m\pi x}{a} e^{j\omega t} \tag{17}$$

$$H_x = \text{Re} \sum_{\substack{m=1 \\ \text{odd}}}^{\infty} \frac{4\beta_m \hat{\Lambda}}{\mu m\pi} \frac{\cos\beta_m y}{\sin\beta_m b} \sin\frac{m\pi x}{a} e^{j\omega t} \tag{18}$$

$$H_y = \text{Re} \sum_{\substack{m=1 \\ \text{odd}}}^{\infty} \frac{-4\hat{\Lambda}}{\mu a} \frac{\sin\beta_m y}{\sin\beta_m b} \cos\frac{m\pi x}{a} e^{j\omega t} \tag{19}$$

In the quasistatic limit, $\omega^2\mu\epsilon \ll (m\pi/a)^2$, this magnetic field reduces to that found in Example 8.6.3.

A few observations may help one to gain some insights from these expressions. First, if the magnetic field is sensed, then the detection loop must have its axis in the $x - y$ plane. For these TE modes, there should be no signal sensed with the axis of the detection loop in the z direction. This probe can also be used to verify that **H** normal to the perfectly conducting surfaces is indeed zero, while its tangential value peaks at the short. Second, the same decay of the fields below cutoff and appearance of standing waves above cutoff is predicted here, as in the TM case. Third, because **E** is perpendicular to planes of constant z, the boundary conditions on **E**, and hence **H**, are met, even if perfectly conducting plates are placed over the open ends of the guide, say in the planes $z = 0$ and $z = w$. In this case, the guide becomes a closed pipe of rectangular cross-section. What we have found are then a subset of the three-dimensional modes of propagation in a rectangular waveguide.

Demonstration 13.3.2.   Evanescent and Standing TE Waves

The apparatus of Demonstration 13.3.1 is altered to give TE rather than TM waves by using an array of "one-turn inductors" rather than the array of "capacitor plates." These are shown in Fig. 13.3.6.
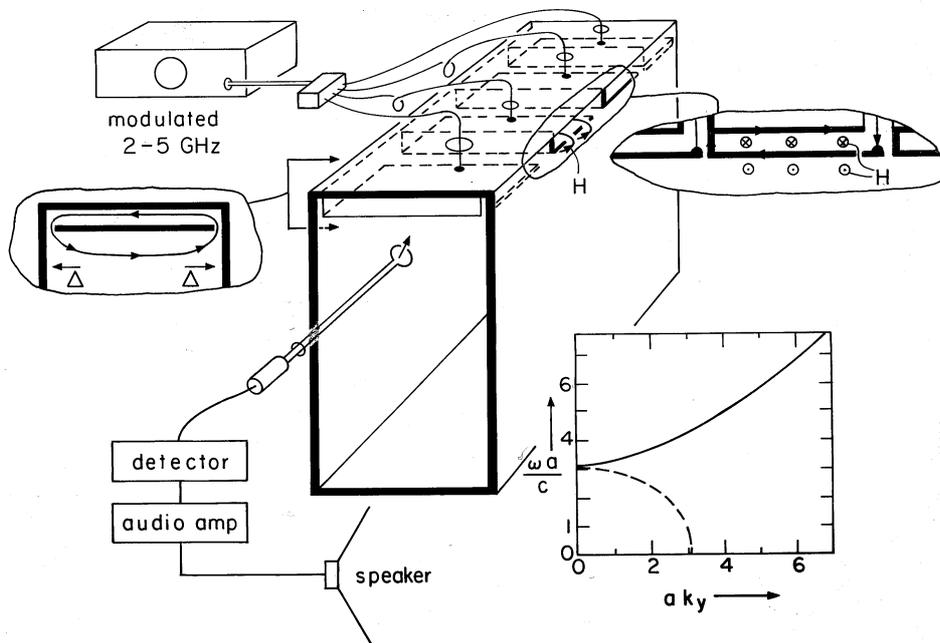
Fig. 13.3.6   Demonstration of evanescent and standing TE waves.

Each member of the array consists of an electrode of width $a - 2\Delta$, driven at one edge by a common source and shorted to the perfectly conducting backing at its other edge. Thus, the magnetic flux through the closed loop passes into and out of the guide through the gaps of width Δ between the ends of the one-turn coil and the parallel plate (vertical) walls of the guide. Effectively, the integral of E_z created by the voltage sources in the idealized model of Fig. 13.3.4 is produced by the integral of E_z between the left edge of one current loop and the right edge of the next.

The current loop can be held in the $x - z$ plane to sense H_y or in the $y - z$ plane to sense H_x to verify the field distributions derived in the previous example. It can also be observed that placing conducting sheets against the open ends of the parallel plate guide, making it a rectangular pipe guide, leaves the characteristics of these two-dimensional TE modes unchanged.

13.4 RECTANGULAR WAVEGUIDE MODES

Metal pipe waveguides are often used to guide electromagnetic waves. The most common waveguides have rectangular cross-sections and so are well suited for the exploration of electrodynamic fields that depend on three dimensions. Although we confine ourselves to a rectangular cross-section and hence Cartesian coordinates, the classification of waveguide modes and the general approach used here are equally applicable to other geometries, for example to waveguides of circular cross-section.

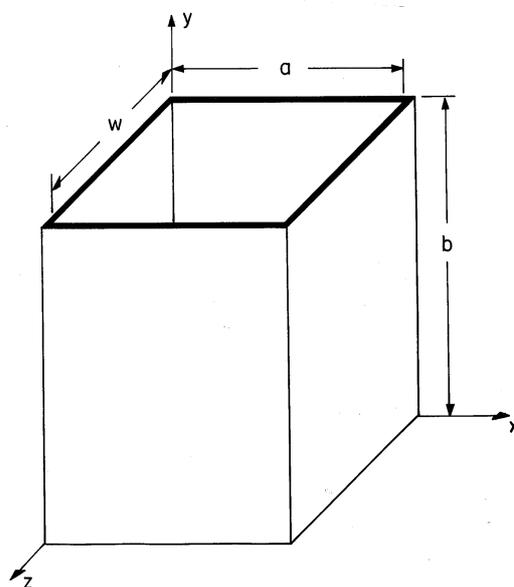The parallel plate system considered in the previous three sections illustrates

Fig. 13.4.1   Rectangular waveguide.

much of what can be expected in pipe waveguides. However, unlike the parallel plates, which can support TEM modes as well as higher-order TE modes and TM modes, the pipe cannot transmit a TEM mode. From the parallel plate system, we expect that a waveguide will support *propagating* modes only if the frequency is high enough to make the greater interior cross-sectional dimension of the pipe greater than a free space half-wavelength. Thus, we will find that a guide having a larger dimension greater than 5 cm would typically be used to guide energy having a frequency of 3 GHz.

   We found it convenient to classify two-dimensional fields as transverse magnetic (TM) or transverse electric (TE) according to whether **E** or **H** was transverse to the direction of propagation (or decay). Here, where we deal with three-dimensional fields, it will be convenient to classify fields according to whether they have **E** or **H** *transverse to the axial direction of the guide*. This classification is used regardless of the cross-sectional geometry of the pipe. We choose again the y coordinate as the axis of the guide, as shown in Fig. 13.4.1. If we focus on solutions to Maxwell's equations taking the form

$$H_y = \text{Re } \hat{h}_y(x, z)e^{j(\omega t - k_y y)} \tag{1}$$

$$E_y = \text{Re } \hat{e}_y(x, z)e^{j(\omega t - k_y y)} \tag{2}$$

then all of the other complex amplitude field components can be written in terms of the complex amplitudes of these axial fields, H_y and E_y. This can be seen from substituting fields having the form of (1) and (2) into the transverse components of Ampère's law, (12.0.8),

$$-jk_y\hat{h}_z - \frac{\partial \hat{h}_y}{\partial z} = j\omega\epsilon\hat{e}_x \tag{3}$$

$$\frac{\partial \hat{h}_y}{\partial x} + jk_y\hat{h}_x = j\omega\epsilon\hat{e}_z \tag{4}$$

and into the transverse components of Faraday's law, (12.0.9),

$$-jk_y\hat{e}_z - \frac{\partial \hat{e}_y}{\partial z} = -j\omega\mu\hat{h}_x \tag{5}$$

$$\frac{\partial \hat{e}_y}{\partial x} + jk_y\hat{e}_x = -j\omega\mu\hat{h}_z \tag{6}$$

If we take $\hat{h}_y$ and $\hat{e}_y$ as specified, (3) and (6) constitute two algebraic equations in the unknowns $\hat{e}_x$ and $\hat{h}_z$. Thus, they can be solved for these components. Similarly, $\hat{h}_x$ and $\hat{e}_z$ follow from (4) and (5).

$$\hat{h}_x = \left(- jk_y\frac{\partial \hat{h}_y}{\partial x} - j\omega\epsilon\frac{\partial \hat{e}_y}{\partial z} \right)/(\omega^2\mu\epsilon - k_y^2) \tag{7}$$

$$\hat{h}_z = \left(- jk_y\frac{\partial \hat{h}_y}{\partial z} + j\omega\epsilon\frac{\partial \hat{e}_y}{\partial x} \right)/(\omega^2\mu\epsilon - k_y^2) \tag{8}$$

$$\hat{e}_x = \left(j\omega\mu\frac{\partial \hat{h}_y}{\partial z} - jk_y\frac{\partial \hat{e}_y}{\partial x} \right)/(\omega^2\mu\epsilon - k_y^2) \tag{9}$$

$$\hat{e}_z = \left(- j\omega\mu\frac{\partial \hat{h}_y}{\partial x} - jk_y\frac{\partial \hat{e}_y}{\partial z} \right)/(\omega^2\mu\epsilon - k_y^2) \tag{10}$$

We have found that the three-dimensional fields are a superposition of those associated with E_y (so that the magnetic field is transverse to the guide axis), the TM fields, and those due to H_y, the TE modes. The axial field components now play the role of "potentials" from which the other field components can be derived.

We can use the y components of the laws of Ampère and Faraday together with Gauss' law and the divergence law for **H** to show that the axial complex amplitudes $\hat{e}_y$ and $\hat{h}_y$ satisfy the two-dimensional Helmholtz equations.

TM Modes $(H_y = 0)$:

$$\frac{\partial^2 \hat{e}_y}{\partial x^2} + \frac{\partial^2 \hat{e}_y}{\partial z^2} + p^2\hat{e}_y = 0 \tag{11}$$

where

$$p^2 = \omega^2\mu\epsilon - k_y^2$$

and

TE Modes $(E_y = 0)$:

$$\frac{\partial^2 \hat{h}_y}{\partial x^2} + \frac{\partial^2 \hat{h}_y}{\partial z^2} + q^2\hat{h}_y = 0 \tag{12}$$

where

$$q^2 = \omega^2 \mu \epsilon - k_y^2$$

These relations also follow from substitution of (1) and (2) into the y components of (13.0.2) and (13.0.1).

The solutions to (11) and (12) must satisfy boundary conditions on the perfectly conducting walls. Because E_y is parallel to the perfectly conducting walls, it must be zero there.

TM Modes:

$$\hat{e}_y(0, z) = 0; \quad \hat{e}_y(a, z) = 0; \quad \hat{e}_y(x, 0) = 0; \quad \hat{e}_y(x, w) = 0 \tag{13}$$

The boundary condition on H_y follows from (9) and (10), which express $\hat{e}_x$ and $\hat{e}_z$ in terms of $\hat{h}_y$. On the walls at $x = 0$ and $x = a$, $\hat{e}_z = 0$. On the walls at $z = 0$, $z = w$, $\hat{e}_x = 0$. Therefore, from (9) and (10) we obtain

TE Modes:

$$\frac{\partial h_y}{\partial x}(0, z) = 0; \quad \frac{\partial h_y}{\partial x}(a, z) = 0; \quad \frac{\partial h_y}{\partial z}(x, 0) = 0; \quad \frac{\partial h_y}{\partial z}(x, w) = 0 \tag{14}$$

The derivative of $\hat{h}_y$ with respect to a coordinate perpendicular to the boundary must be zero.

The solution to the Helmholtz equation, (11) or (12), follows a pattern that is familiar from that used for Laplace's equation in Sec. 5.4. Either of the complex amplitudes representing the axial fields is represented by a product solution.

$$\begin{bmatrix} \hat{e}_y \\ \hat{h}_y \end{bmatrix} \propto X(x)Z(z) \tag{15}$$

Substitution into (11) or (12) and separation of variables then gives

$$\frac{d^2 X}{dx^2} + \gamma^2 X = 0 \tag{16}$$

$$\frac{d^2 Z}{dz^2} + \delta^2 Z = 0$$

where

$$-\gamma^2 - \delta^2 + \begin{pmatrix} p^2 \\ q^2 \end{pmatrix} = 0 \tag{17}$$

Solutions that satisfy the TM boundary conditions, (13), are then

TM Modes:

$$X \propto \sin \gamma_m x; \qquad \gamma_m = \frac{m\pi}{a}, \quad m = 1, 2, \ldots \tag{18}$$

$$Z \propto \sin \delta_n z; \qquad \delta_n = \frac{n\pi}{w}, \quad n = 1, 2, \ldots$$

so that

$$p_{mn}^2 = \left(\frac{m\pi}{a}\right)^2 + \left(\frac{n\pi}{w}\right)^2; \qquad m = 1, 2, \ldots, \quad n = 1, 2, \ldots \tag{19}$$

When either m or n is zero, the field is zero, and thus m and n must be equal to an integer equal to or greater than one. For a given frequency ω and mode number (m, n), the wave number k_y is found by using (19) in the definition of p associated with (11)

$$k_y = \pm \beta_{mn}$$

with

$$\beta_{mn} \equiv \begin{cases} \sqrt{\omega^2 \mu\epsilon - \left(\frac{m\pi}{a}\right)^2 - \left(\frac{n\pi}{w}\right)^2}; & \omega^2 \mu\epsilon > \left(\frac{m\pi}{a}\right)^2 + \left(\frac{n\pi}{w}\right)^2 \\ -j\sqrt{\left(\frac{m\pi}{a}\right)^2 + \left(\frac{n\pi}{w}\right)^2 - \omega^2 \mu\epsilon}; & \omega^2 \mu\epsilon < \left(\frac{m\pi}{a}\right)^2 + \left(\frac{n\pi}{w}\right)^2 \end{cases} \tag{20}$$

Thus, the TM solutions are

$$E_y = \mathrm{Re} \sum_{m=1}^{\infty} \sum_{n=1}^{\infty} (A_{mn}^+ e^{-j\beta_{mn}y} + A_{mn}^- e^{j\beta_{mn}y}) \sin \frac{m\pi}{a} x \, \sin \frac{n\pi}{w} z \, e^{j\omega t} \tag{21}$$

For the TE modes, (14) provides the boundary conditions, and we are led to the solutions

TE Modes:

$$X \propto \cos \gamma_m x; \qquad \gamma_m = \frac{m\pi}{a}; \quad m = 0, 1, 2, \ldots \tag{22}$$

$$Z \propto \cos \delta_n z; \qquad \delta_n = \frac{n\pi}{a}; \quad n = 0, 1, 2, \ldots$$

Substitution of γ_m and δ_n into (17) therefore gives

$$q_{mn}^2 = \left(\frac{m\pi}{a}\right)^2 + \left(\frac{n\pi}{w}\right)^2; \qquad m = 0, 1, 2, \ldots, \quad n = 0, 1, 2, \ldots, \tag{23}$$

$$(m, n) \neq (0, 0)$$

The wave number k_y is obtained using this eigenvalue in the definition of q associated with (12). With the understanding that either m or n can now be zero, the expression is the same as that for the TM modes, (20). However, both m and n cannot be zero. If they were, it follows from (22) that the axial **H** would be uniform over any given cross-section of the guide. The integral of Faraday's law over the cross-section of the guide, with the enclosing contour C adjacent to the perfectly conducting boundaries as shown in Fig. 13.4.2, requires that

$$\oint \mathbf{E} \cdot d\mathbf{s} = -\mu A \frac{dH_y}{dt} \tag{24}$$
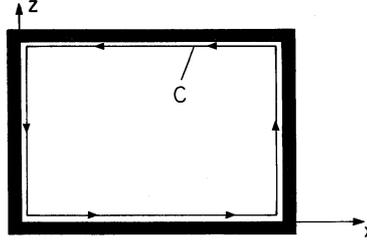
Fig. 13.4.2 Cross-section of guide with contour adjacent to perfectly conducting walls.

where A is the cross-sectional area of the guide. Because the contour on the left is adjacent to the perfectly conducting boundaries, the line integral of $\mathbf{E}$ must be zero. It follows that for the $m = 0$, $n = 0$ mode, $H_y = 0$. If there were such a mode, it would have both $\mathbf{E}$ and $\mathbf{H}$ transverse to the guide axis. We will show in Sec. 14.2, where TEM modes are considered in general, that TEM modes cannot exist within a perfectly conducting pipe.

Even though the dispersion equations for the TM and TE modes only differ in the allowed lowest values of (m, n), the field distributions of these modes are very different.[9] The superposition of TE modes gives

$$H_y = \text{Re} \sum_{m=0}^{\infty} \sum_{n=0}^{\infty} (C_{mn}^{+} e^{-j\beta_{mn}y} + C_{mn}^{-} e^{j\beta_{mn}y}) \cdot \cos \frac{m\pi}{a} x \, \cos \frac{n\pi}{w} z \, e^{j\omega t} \qquad (25)$$

where $m \cdot n \neq 0$. The frequency at which a given mode switches from evanescence to propagation is an important parameter. This *cutoff frequency* follows from (20) as

$$\omega_c = \frac{1}{\sqrt{\mu\epsilon}} \sqrt{\left(\frac{m\pi}{a}\right)^2 + \left(\frac{n\pi}{w}\right)^2} \qquad (26)$$

TM Modes:

$$m \neq 0, \quad n \neq 0$$

TE Modes:

$$m \quad \text{and} \quad n \quad \text{not both zero}$$

Rearranging this expression gives the normalized cutoff frequency as functions of the aspect ratio a/w of the guide.

$$\underline{\omega}_c \equiv \frac{\omega_c w}{c\pi} = \sqrt{(w/a)^2 m^2 + n^2} \qquad (27)$$

These normalized cutoff frequencies are shown as functions of w/a in Fig. 13.4.3.

The numbering of the modes is standardized. The dimension w is chosen as $w \leq a$, and the first index m gives the variation of the field along a. The TE_{10}

---

[9] In other geometries, such as a circular waveguide, this coincidence of p_{mn} and q_{mn} is not found.
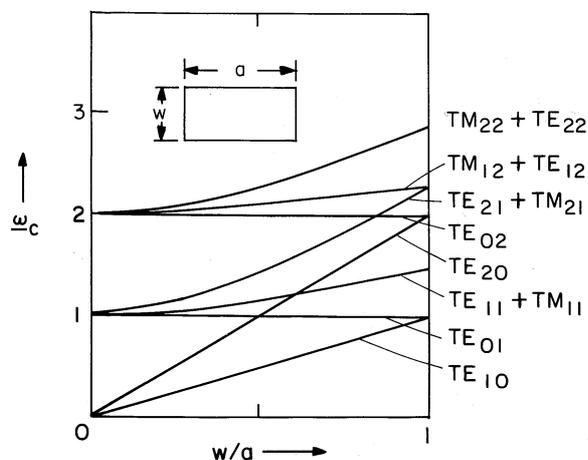
Fig. 13.4.3 Normalized cutoff frequencies for lowest rectangular waveguide modes as a function of aspect ratio.

mode then has the lowest cutoff frequency and is called the *dominant* mode. All other modes have higher cutoff frequencies (except, of course, in the case of the square cross-section for which TE_{01} has the same cutoff frequency). Guides are usually designed so that at the frequency of operation only the dominant mode is propagating, while all higher-order modes are "cutoff."

In general, an excitation of the guide at a cross-section $y = $ constant excites all waveguide modes. The modes with cutoff frequencies higher than the frequency of excitation decay away from the source. Only the dominant mode has a sinusoidal dependence upon y and thus possesses fields that are periodic in y and "dominate" the field pattern far away from the source, at distances larger than the transverse dimensions of the waveguide.

Example 13.4.1. TE_{10} Standing Wave Fields

The section of rectangular guide shown in Fig. 13.4.4 is excited somewhere to the right of $y = 0$ and shorted by a conducting plate in the plane $y = 0$. We presume that the frequency is above the cutoff frequency for the TE_{10} mode and that $a > w$ as shown. The frequency of excitation is chosen to be below the cutoff frequency for all higher order modes and the source is far away from $y = 0$ (i.e., at $y \gg a$). The field in the guide is then that of the TE_{10} mode. Thus, H_y is given by (25) with $m = 1$ and $n = 0$. What is the space-time dependence of the standing waves that result from having shorted the guide?

Because of the short, $E_z(x, y = 0, z) = 0$. In order to relate the coefficients C_{10}^+ and C_{10}^-, we must determine $\hat{e}_z$ from $\hat{h}_y$ as given by (25) using (10)

$$E_z = \text{Re } j\omega\mu \frac{a}{\pi}(C_{10}^+ e^{-j\beta_{10}y} + C_{10}^- e^{j\beta_{10}y}) \sin \frac{\pi x}{a} e^{j\omega t} \tag{28}$$

and because $\hat{e}_z = 0$ at the short, it follows that
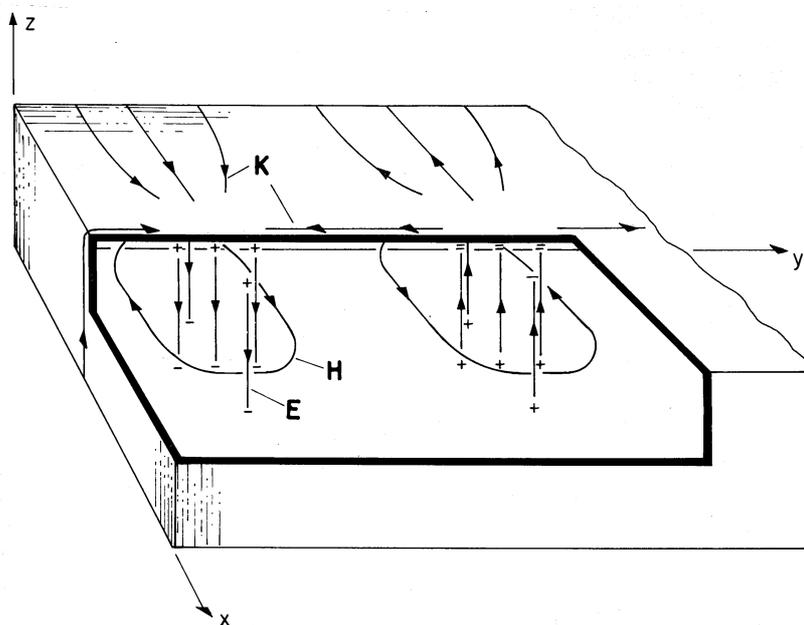
$$C_{10}^+ = -C_{10}^- \tag{29}$$

Fig. 13.4.4   Fields and surface sources for TE$_{10}$ mode.

so that

$$E_z = \text{Re}\left[2\omega\mu\frac{a}{\pi}C_{10}^+ \sin\beta_{10}y \sin\frac{\pi}{a}x e^{j\omega t}\right] \tag{30}$$

and this is the only component of the electric field in this mode. We can now use (29) to evaluate (25).

$$H_y = -\text{Re}\left[2jC_{10}^+ \sin\beta_{10}y \cos\frac{\pi}{a}x e^{j\omega t}\right] \tag{31}$$

In using (7) to evaluate the other component of **H**, remember that in the C_{mn}^+ term of (25), $k_y = \beta_{mn}$, while in the C_{mn}^- term, $k_y = -\beta_{mn}$.

$$H_x = \text{Re}\left[2j\beta_{10}\frac{a}{\pi}C_{10}^+ \cos\beta_{10}y \sin\frac{\pi}{a}x e^{j\omega t}\right] \tag{32}$$

   To sketch these fields in the neighborhood of the short and deduce the associated surface charge and current densities, consider C_{10}^+ to be real. The j in (31) and (32) shows that H_x and H_y are 90 degrees out of phase with the electric field. Thus, in the field sketches of Fig. 13.4.4, **E** and **H** are shown at different instants of time, say **E** when $\omega t = \pi$ and **H** when $\omega t = \pi/2$. The surface charge density is where E_z terminates and originates on the upper and lower walls. The surface current density can be inferred from Ampère's continuity condition. The temporal oscillations of these fields should be pictured with **H** equal to zero when **E** peaks, and with **E** equal to zero when **H** peaks. At planes spaced by multiples of a half-wavelength along the y axis, **E** is always zero.
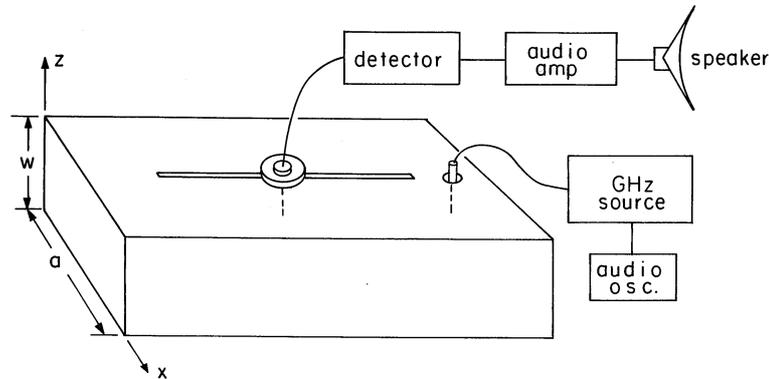
Fig. 13.4.5   Slotted line for measuring axial distribution of TE_{10} fields.

The following demonstration illustrates how a movable probe designed to couple to the electric field is introduced into a waveguide with minimal disturbance of the wall currents.

Demonstration 13.4.1.   Probing the TE_{10} Mode.

A waveguide slotted line is shown in Fig. 13.4.5. Here the line is shorted at $y = 0$ and excited at the right. The probe used to excite the guide is of the capacitive type, positioned so that charges induced on its tip couple to the lines of electric field shown in Fig. 13.4.4. This electrical coupling is an alternative to the magnetic coupling used for the TE mode in Demonstration 13.3.2.

The y dependence of the field pattern is detected in the apparatus shown in Fig. 13.4.5 by means of a second capacitive electrode introduced through a slot so that it can be moved in the y direction and not perturb the field, i.e., the wall is cut *along* the lines of the surface current $\mathbf{K}$. From the sketch of $\mathbf{K}$ given in Fig. 13.4.4, it can be seen that $\mathbf{K}$ is in the y direction along the center line of the guide.

The probe can be used to measure the wavelength $2\pi/k_y$ of the standing waves by measuring the distance between nulls in the output signal (between nulls in E_z). With the frequency somewhat below the cutoff of the TE_{10} mode, the spatial decay away from the source of the evanescent wave also can be detected.

13.5 DIELECTRIC WAVEGUIDES: OPTICAL FIBERS

Waves can be guided by dielectric rods or slabs and the fields of these waves occupy the space within and around these dielectric structures. Especially at optical wavelengths, dielectric fibers are commonly used to guide waves. In this section, we develop the properties of waves guided by a planar sheet of dielectric material. The waves that we find are typical of those found in integrated optical systems and in the more commonly used optical fibers of circular cross-section.

A planar version of a dielectric waveguide is pictured in Fig. 13.5.1. A dielectric of thickness $2d$ and permittivity ϵ_i is surrounded by a dielectric of permittivity $\epsilon < \epsilon_i$. The latter might be free space with $\epsilon = \epsilon_o$. We are interested in how this
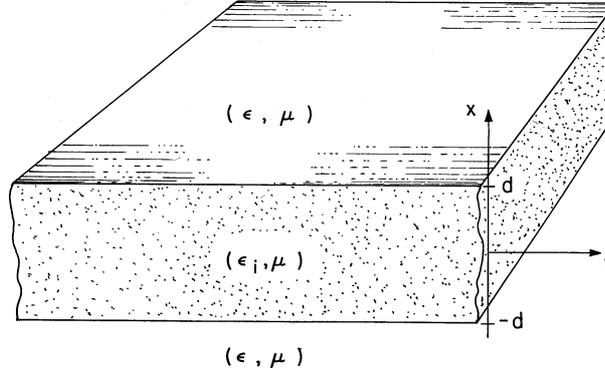
Fig. 13.5.1   Dielectric slab waveguide.

structure might be used to guide waves in the y direction and will confine ourselves to fields that are independent of z.

With a source somewhere to the left (for example an antenna imbedded in the dielectric), there is reason to expect that there are fields outside as well as inside the dielectric. We shall look for field solutions that propagate in the y direction and possess fields solely inside and near the layer. The fields external to the layer decay to zero in the $\pm x$ directions. Like the waves propagating along waveguides, those guided by this structure have transverse components that take the form

$$E_z = \text{Re } \hat{e}_z(x)e^{j(\omega t - k_y y)} \tag{1}$$

both inside and outside the dielectric. That is, the fields inside and outside the dielectric have the same frequency ω, the same phase velocity ω/k_y, and hence the same wavelength $2\pi/k_y$ in the y direction. Of course, whether such fields can actually exist will be determined by the following analysis.

The classification of two-dimensional fields introduced in Sec. 12.6 is applicable here. The TM and TE fields can be made to independently satisfy the boundary conditions so that the resulting modes can be classified as TM or TE.[10] Here we will confine ourselves to the transverse electric modes. In the exterior and interior regions, where the permittivities are uniform but different, it follows from substitution of (1) into (12.6.33) (Table 12.8.3) that

$$\frac{d^2\hat{e}_z}{dx^2} - \alpha_x^2\hat{e}_z = 0; \qquad \alpha_x = \sqrt{k_y^2 - \omega^2\mu\epsilon}; \quad d < x \text{ and } x < -d \tag{2}$$

$$\frac{d^2\hat{e}_z}{dx^2} + k_x^2\hat{e}_z = 0; \qquad k_x = \sqrt{\omega^2\mu\epsilon_i - k_y^2}; \quad -d < x < d \tag{3}$$

A guided wave is one that is composed of a nonuniform plane wave in the exterior regions, decaying in the $\pm x$ directions and propagating with the phase velocity ω/k_y in the y direction. In anticipation of this, we have written (2) in

---

[10] Circular dielectric rods do not support simple TE or TM waves; in that case, this classification of modes is not possible.

terms of the parameter α_x, which must then be real and positive. Through the continuity conditions, the exterior wave must match up to the interior wave at the dielectric surfaces. The solutions to (3) are sines and cosines if k_x is real. In order to match the interior fields onto the nonuniform plane waves on both sides of the guide, it is necessary that k_x be real.

We now set out to find the wave numbers k_y that not only satisfy the wave equations in each of the regions, represented by (2) and (3), but the continuity conditions at the interfaces as well. The configuration is symmetric about the $x = 0$ plane so we can further divide the modes into those that have even and odd functions $E_z(x)$. Thus, with A an arbitrary factor, appropriate even solutions to (2) and (3) are

$$\hat{e}_z = \begin{cases} Ae^{-\alpha_x(x-d)}; & d < x \\ A\dfrac{\cos k_x x}{\cos k_x d}; & -d < x < d \\ Ae^{\alpha_x(x+d)}; & x < -d \end{cases} \tag{4}$$

To simplify the algebra, we have displaced the origin in the exterior solutions so that just the coefficient, A, is obtained when $\hat{e}_z$ is evaluated at the respective interfaces. With a similar objective, the interior solution has been divided by the constant $\cos(k_x d)$ so that at the boundaries, $\hat{e}_z$ also becomes A. In this way, we have adjusted the interior coefficient so that $\hat{e}_z$ is continuous at the boundaries.

Because this transverse field is the only component of $\mathbf{E}$, all of the continuity conditions on $\mathbf{E}$ are now satisfied. The permeabilities of all regions are presumed to be the same, so both tangential and normal components of $\mathbf{H}$ must be continuous at the boundaries. From (12.6.29), the continuity of normal $\mu\mathbf{H}$ is guaranteed by the continuity of E_z in any case. The tangential field is obtained using (12.6.30).

$$\hat{h}_y = \frac{1}{j\omega\mu}\frac{d\hat{e}_z}{dx} \tag{5}$$

Substitution of (4) into (5) gives

$$\hat{h}_y = \frac{1}{j\omega\mu}\begin{cases} -\alpha_x Ae^{-\alpha_x(x-d)}; & d < x \\ -k_x A\frac{\sin k_x x}{\cos k_x d}; & -d < x < d \\ \alpha_x Ae^{\alpha_x(x+d)}; & x < -d \end{cases} \tag{6}$$

The assumption that E_z is even in x has as a consequence the fact that the continuity condition on tangential $\mathbf{H}$ is satisfied by the same relation at both boundaries.

$$-\alpha_x A = -k_x A \tan k_x d \Rightarrow \frac{\alpha_x}{k_x} = \tan k_x d \tag{7}$$

Our goal is to determine the propagation constant k_y for a given ω. If we were to substitute the definitions of α_x and k_x into this expression, we would have this dispersion equation, $D(\omega, k_y)$, implicitly relating k_y to ω. It is more convenient to solve for α_x and k_x first, and then for k_y.

Elimination of k_y between the expressions for α_x and k_x given with (2) and (3) gives a second expression for α_x/k_x.

$$\frac{\alpha_x}{k_x} = \sqrt{\frac{\omega^2 \mu\epsilon_i d^2}{(k_x d)^2}\left(1 - \frac{\epsilon}{\epsilon_i}\right) - 1} \tag{8}$$
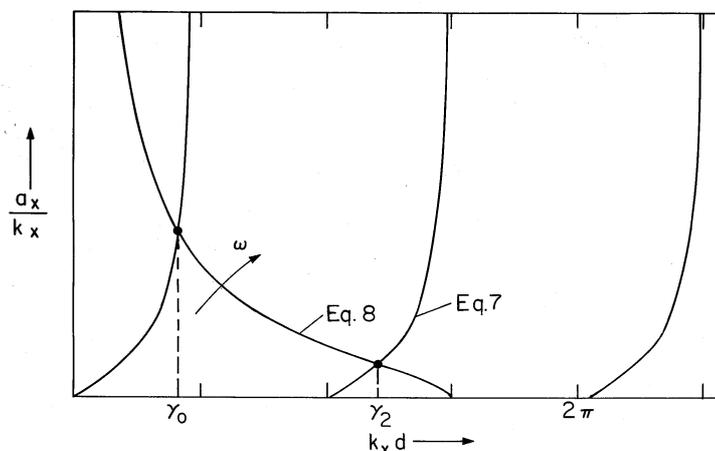
Fig. 13.5.2 Graphical solution to (7) and (8).

The solutions for the values of the normalized transverse wave numbers $(k_x d)$ can be pictured as shown in Fig. 13.5.2. Plotted as functions of $k_x d$ are the right-hand sides of (7) and (8). The points of intersection, $k_x d = \gamma_m$, are the desired solutions. For the frequency used to make Fig. 13.5.2, there are two solutions. These are designated by even integers because the odd modes (Prob. 13.5.1) have roots that interleave these even modes.

As the frequency is raised, an additional even TE-guided mode is found each time the curve representing (8) reaches a new branch of (7). This happens at frequencies ω_c such that $\alpha_x/k_x = 0$ and $k_x d = m\pi/2$, where $m = 0, 2, 4, \ldots$ From (8),

$$\omega_c = \frac{m\pi}{2d} \frac{1}{\sqrt{\mu(\epsilon_i - \epsilon)}} \tag{9}$$

The $m = 0$ mode has no cutoff frequency.

To finally determine k_y from these eigenvalues, the definition of k_x given with (3) is used to write

$$k_y d = \sqrt{\omega^2 \mu \epsilon_i d^2 - (k_x d)^2} \tag{10}$$

and the dispersion equation takes the graphical form of Fig. 13.5.3. To make Fig. 13.5.2, we had to specify the ratio of permittivities, so that ratio is also implicit in Fig. 13.5.3.

Features of the dispersion diagram, Fig. 13.5.3, can be gathered rather simply. Where a mode is just cutoff because $\omega = \omega_c$, $\alpha_x = 0$, as can be seen from Fig. 13.5.2. From (2), we gather that $k_y = \omega_c\sqrt{\mu\epsilon}$. Thus, at cutoff, a mode must have a propagation constant k_y that lies on the straight broken line to the left, shown in Fig. 13.5.3. At cutoff, each mode has a phase velocity equal to that of a plane wave in the medium exterior to the layer.

In the high-frequency limit, where ω goes to infinity, we see from Fig. 13.5.2 that $k_x d$ approaches the constant $k_x \to (m+1)\pi/2d$. That is, in (3), k_x becomes a constant even as ω goes to infinity and it follows that in this high frequency limit $k_y \to \omega\sqrt{\mu\epsilon_i}$.
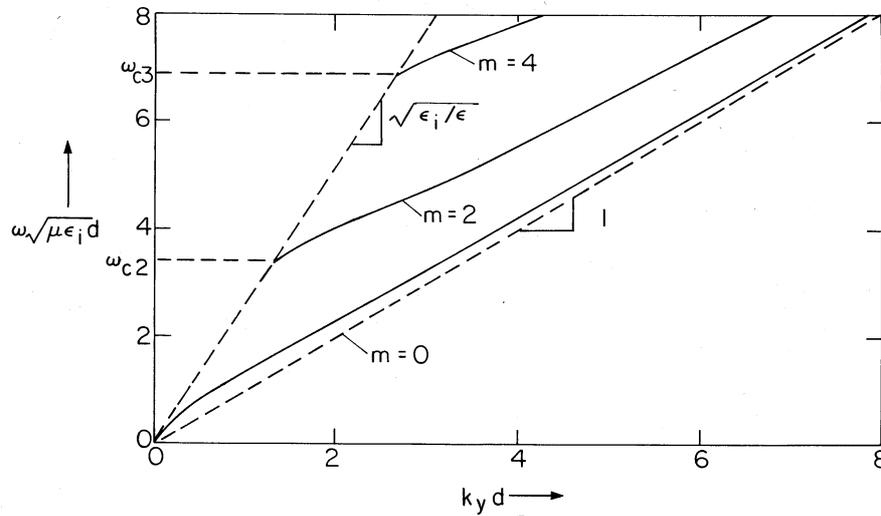
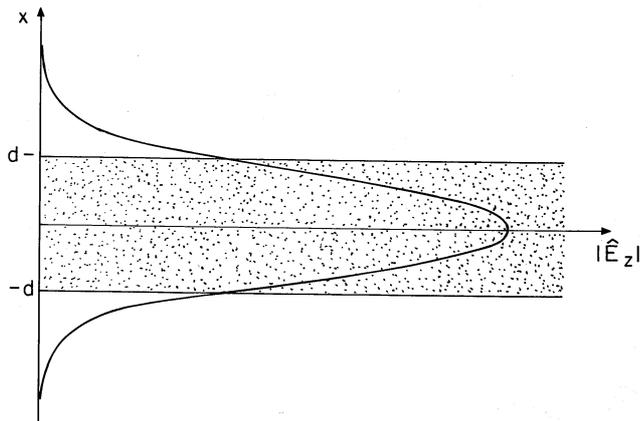**Fig. 13.5.3**   Dispersion equation for even TE modes with $\epsilon_i/\epsilon = 6.6$.

Fig. 13.5.4   Distribution of transverse **E** for TE$_0$ mode on dielectric waveguide of Fig. 13.5.1.

The physical reasons for this behavior follow from the nature of the mode pattern as a function of frequency. When $\alpha_x \to 0$, as the frequency approaches cutoff, it follows from (4) that the fields extend far into the regions outside of the layer. The wave approaches an infinite parallel plane wave having a propagation constant that is hardly affected by the layer. In the opposite extreme, where ω goes to infinity, the decay of the external field is rapid, and a given mode is well confined inside the layer. Again, the wave assumes the character of an infinite parallel plane wave, but in this limit, one that propagates with the phase velocity of a plane wave in a medium with the dielectric constant of the layer.

The distribution of E_z of the $m = 0$ mode at one frequency is shown in Fig. 13.5.4. As the frequency is raised, each mode becomes more confined to the layer.
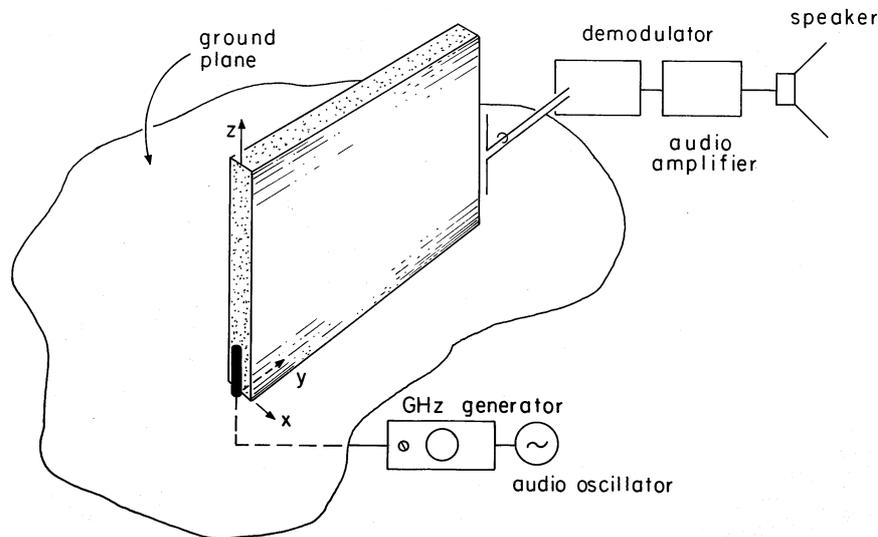
Fig. 13.5.5   Dielectric waveguide demonstration.

Demonstration 13.5.1.   Microwave Dielectric Guided Waves

In the experiment shown in Fig. 13.5.5, a dielectric slab is demonstrated to guide microwaves. To assure the excitation of only an $m = 0$ TE-guided wave, but one as well confined to the dielectric as possible, the frequency is made just under the cutoff frequency ω_{c2}. (For a 2 cm thick slab having $\epsilon_i/\epsilon_o = 6.6$, this is a frequency just under 6 GHz.) The $m = 0$ wave is excited in the dielectric slab by means of a vertical element at its left edge. This assures excitation of E_z while having the symmetry necessary to avoid excitation of the odd modes.

The antenna is mounted at the center of a metal ground plane. Thus, without the slab, the signal at the receiving antenna (which is oriented to be sensitive to E_z) is essentially the same in all directions perpendicular to the z axis. With the slab, a sharply increased signal in the vicinity of the right edge of the slab gives qualitative evidence of the wave guidance. The receiving antenna can also be used to probe the field decay in the x direction and to see that this decay increases with frequency.[11]

13.6 SUMMARY

There are two perspectives from which this chapter can be reviewed. First, it can be viewed as a sequence of specific examples that are useful for dealing with radio frequency, microwave, and optical systems. Secs. 13.1–13.3 are concerned with the propagation of energy along parallel plates, first acting as a transmission line and then as a waveguide. Practical systems to which the derived properties of the TEM and higher-order modes are directly applicable are strip lines used at frequencies

---

[11] To make the excitation independent of z, a collinear array of in-phase dipoles could be used for the excitation. This is not necessary to demonstrate the qualitative features of the guide.

that extend from dc to the microwave range. The rectangular waveguide of Sec. 13.4 might well be a section of "plumbing" from a microwave communication system, and the dielectric waveguide of Sec. 13.5 has many of the properties of an optical fiber. Second, the mathematical analysis of waves exemplified in this chapter is generally applicable to other more complex systems that are uniform in one direction.

When the structures described in this chapter are used to transport energy from one location to another, they are generally not terminated in "shorts" and "opens" and hence, generally, do not simply support standing waves. The object is usually to carry energy from an antenna to a receiver or from a generator to a load whether that be an antenna or a light bulb. Such energy transport is accomplished by the traveling waves featured in the next chapter.

P R O B L E M S

13.1 Introduction to TEM Waves

13.1.1[*] With a short at $y = 0$, it is possible to find the fields for Example 13.1.1 by recognizing at the outset that standing wave solutions meeting the homogeneous boundary condition of (12) are of the form $E_x = \text{Re } A \sin(\beta y) \exp(j\omega t)$.

(a) Use (13.1.2) and (13.1.3) to determine the associated H_z and the dispersion equation (relation between β and ω).
(b) Now use the boundary condition at $y = -b$ to show that the fields are as given by (13.1.16) and (13.1.17).

13.1.2[*] Take the approach outlined in Prob. 13.1.1 for finding the fields [(13.1.28) and (13.1.29)] in Example 13.1.2.

13.1.3 Assume that $\hat{K}_o$ is real and express the standing wave of (13.1.17) so as to make it evident that it is the sum of equal-amplitude waves traveling in the $\pm y$ directions, each with a magnitude of phase velocity $\omega/\beta = c$ and wavelength $2\pi/\beta$.

13.1.4[*] Coaxial perfectly conducting circular cylinders having outer and inner radii a and b, respectively, form the transmission line shown in Fig. P13.1.4.

(a) If the conductors were "open circuit" at $z = 0$ and driven by a voltage source V at $z = -l$, show that the EQS electric field is radial and given by $V/[r\,ln(a/b)]$.
(b) If the conductors were "shorted" at $z = 0$ and driven by a current source I at $z = -l$, show that the MQS magnetic field intensity is ϕ directed and given by $I/2\pi r$.
(c) With the motivation provided by these limiting solutions, show that solutions to all of Maxwell's equations (in the region between the conductors) that satisfy the boundary conditions on the surfaces of the coaxial conductors are

$$\mathbf{E} = \mathbf{i_r}\frac{V(z,t)}{ln\left(\frac{a}{b}\right)r}; \qquad \mathbf{H} = \mathbf{i_\phi}\frac{I(z,t)}{2\pi r} \qquad (a)$$

provided that V and I are now functions not only of t but of z as well that satisfy equations taking the same form as (13.1.2) and (13.1.3).

$$\frac{\partial I}{\partial z} = -C\frac{\partial V}{\partial t}; \qquad C \equiv \frac{2\pi\epsilon}{ln\left(\frac{a}{b}\right)} \qquad (b)$$

$$\frac{\partial V}{\partial z} = -L\frac{\partial I}{\partial t}; \qquad L \equiv \frac{ln\left(\frac{a}{b}\right)\mu}{2\pi} \qquad (c)$$
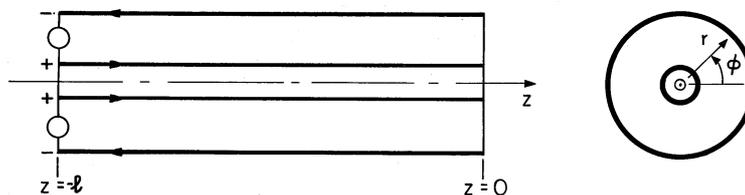
Fig. P13.1.4

13.1.5 For the coaxial configuration of Prob. 13.1.4, there is a perfectly conducting "short" at $z = 0$, and the conductors are driven by a current source $I = \text{Re}[I_o e^{j\omega t}]$ at $z = -l$.

(a) Find $I(z,t)$ and $V(z,t)$ and hence **E** and **H**.
(b) Take the low frequency limit where $\omega \sqrt{\mu \epsilon} l \ll 1$ and show that **E** and **H** are the same as for a coaxial inductor.
(c) Find **E** and **H** directly from the MQS laws and show that they agree with the results of part (b).

13.1.6 For the coaxial configuration of Prob. 13.1.4, the conductors are "open circuited" at $z = 0$ and driven by a voltage source $V = \text{Re}\,[V_o \exp(j\omega t]$ at $x = -l$.

(a) Find $I(z,t)$ and $V(z,t)$ and hence **E** and **H**.
(b) Take the low-frequency limit where $\omega \sqrt{\mu \epsilon} l \ll 1$ and show that **E** and **H** are the same as for a coaxial capacitor.
(c) Find **E** and **H** directly from the EQS laws and show that they agree with the results of (b).

13.2 Two-Dimensional Modes Between Parallel Plates

13.2.1[*] Show that each of the higher-order modes propagating in the $+y$ direction, represented by A_n^+ and C_n^+ in (13.2.19) and (13.2.20), respectively, can be regarded as the sum of plane waves propagating in the directions represented by the vector wave number

$$\mathbf{k} = \pm \frac{n\pi}{a}\mathbf{i_x} + \beta_n \mathbf{i_y} \qquad (a)$$

and interfering in the planes $x = 0$ and $x = a$ so as to satisfy the boundary conditions.

13.2.2 The TM and TE modes can themselves be classified into odd or even modes that, respectively, have $\hat{h}_z$ or $\hat{e}_z$ odd or even functions of x. With this in mind, the origin of the coordinate system is moved so that it is midway between the perfectly conducting plates, as shown in Fig. P13.2.2.
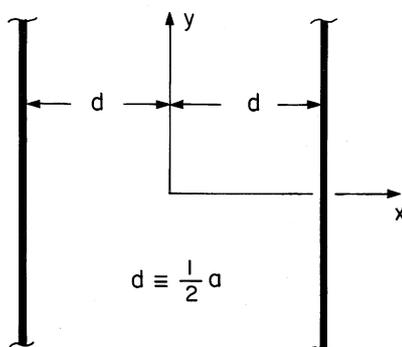
Fig. P13.2.2

(a) Find the odd TM and TE solutions. Note that when the boundary condition is met at $x = d \equiv a/2$ for these functions, it is automatically met at $x = -d$.

(b) Find the even TM and TE solutions, again noting that if the conditions are met at $x = d$, then they are at $x = -d$ as well.

13.3 TE and TM Standing Waves between Parallel Plates

13.3.1* Starting with (13.3.1) (for TM modes) and (13.3.2) (for TE modes) use steps similar to those illustrated by (5.5.20)–(5.5.26) to obtain the orthogonality conditions of (13.3.3) and (13.3.4), respectively.

13.3.2 In the system of Example 13.3.1, the wall at $y = 0$ is replaced by that shown in Fig. P13.3.2. A strip electrode is embedded in, but insulated from, the wall at $y = 0$. The resistance R is low enough so that $\mathbf{E}$ tangential to the boundary at $y = 0$, even at the insulating gaps between the strip electrode and the surrounding wall, is negligible.

(a) Determine the output voltage v_o in terms of v.

(b) For $b/a = 2$, describe the dependence of $|v_o|$ on frequency over the range $\omega\sqrt{\mu\epsilon}\,a = 0 \rightarrow \pi\sqrt{5/4}$, specifying the low-frequency range where the response has a linear dependence on frequency and the resonance frequencies.

(c) What is the distribution of $H_z(x, y)$ at the resonance frequencies?

13.3.3* In the two-dimensional system of Fig. P13.3.3, each driven electrode has the same nature as the one in Fig. 13.3.1. The origin of the y axis has been chosen to be in the plane of symmetry.

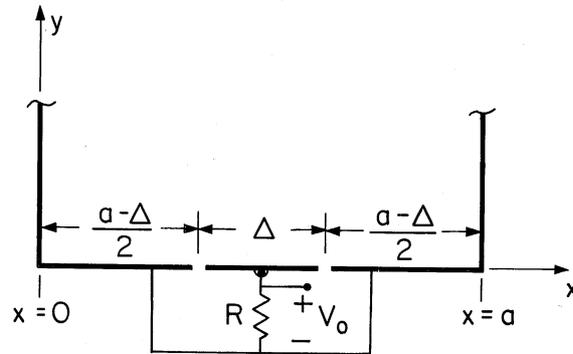(a) Use the symmetry to argue that $H_z(y = 0) = 0$.
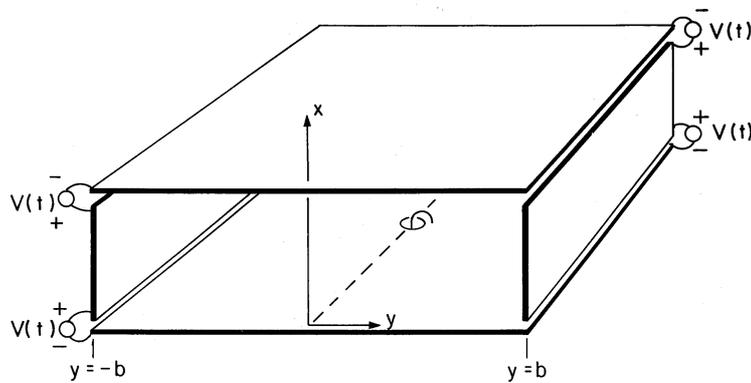
Fig. P13.3.2

Fig. P13.3.3

(b) Show that in the interior region,

$$H_z = \text{Re} \sum_{\substack{n=1 \\ \text{odd}}}^{\infty} \frac{-4j\omega\epsilon\hat{v}}{\beta_n a} \frac{\sin\beta_n y}{\cos\beta_n b} \cos\frac{n\pi x}{a} e^{j\omega t} \qquad (a)$$

13.3.4 The one-turn loop of Fig. P13.3.4 has dimensions that are small compared to a, b, or wavelengths of interest and has area A in the $x - y$ plane.

(a) It is used to detect the TM H field at the middle of the bottom electrode in Fig. 13.3.1. Assume that the resistance is large enough so that the current induced in this loop gives rise to a magnetic field that is negligible compared to that already found. In terms of H_z, what is v_o?

(b) At what locations $x = X$ of the loop is $|v_o|$ a maximum?

(c) If the same loop were in the plate at $y = 0$ in the configuration of Fig. 13.1.3 and used to detect H_z at $y = 0$ for the TEM fields of Example
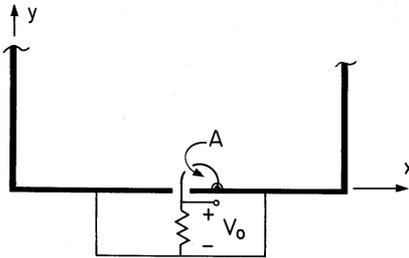
Fig. P13.3.4

13.1.1, what would be the dependence of $|v_o|$ on the location $x = X$ of the loop?

(d) If the loop were located in the plate at $y = 0$ in the TE configuration of Fig. 13.3.4, how should the loop be oriented to detect **H**?

13.3.5 In the system shown in Fig. P13.3.5, $\Delta \ll d$ and the driving sources $v = \mathrm{Re}[\hat{v}\exp(j\omega t)]$ are uniformly distributed in the z direction so that the fields are two dimensional. Thus, the driving electrode is like that of Fig. 13.3.1 except that it spans the width d rather than the full width a. Find **H** and **E** in terms of v.

13.3.6 In the system shown in Fig. P13.3.6, the excitation electrode is like that for Fig. 13.3.4 except that it has a width d rather than a. Find **H** and **E** in terms of $\hat{\Lambda}$.

13.4 Rectangular Waveguide Modes

13.4.1[*] Show that an alternative method of exciting and detecting the TE_{10} mode in Demonstration 13.4.1 is to introduce one-turn loops as shown in Fig. P13.4.1. The excitation loop is inserted through a hole in the conducting wall while the detection loop passes through a slot, so that it can be moved in the y direction. The loops are each in the $y - z$ plane. To minimize disturbance of the field, the detection loop is terminated in a high enough impedance so that the field from the current in the loop is negligible. Compare the y dependence of the detected signal to that measured using the electric probe.

13.4.2 A rectangular waveguide has $w/a = 0.75$. Presuming that all TE and TM modes are excited in the guide, in what order do the lowest six modes begin to propagate in the y direction as the frequency is raised?

13.4.3[*] The rectangular waveguide shown in Fig. P13.4.3 is terminated in a perfectly conducting plate at $y = 0$ that makes contact with the guide walls. An electrode at $y = b$ has a gap of width $\Delta \ll a$ and $\Delta \ll w$ around its
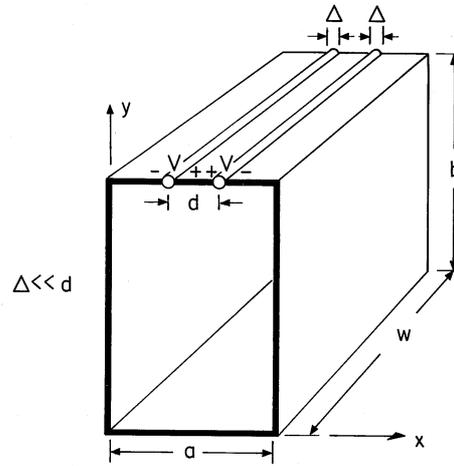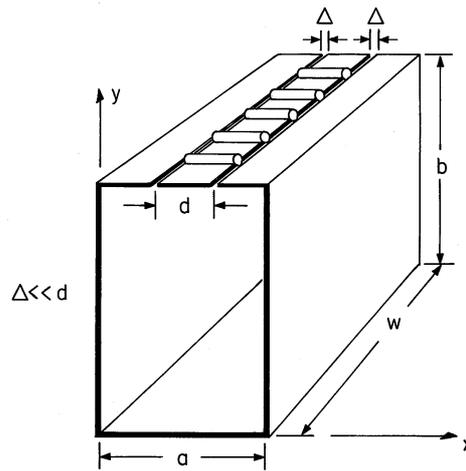
Fig. P13.3.5

Fig. P13.3.6

Fig. P13.4.1

edges. Distributed around this gap are sources that constrain the field from the edges of the plate to the guide walls to $v(t)/\Delta = \mathrm{Re}(\hat{v}/\Delta)\exp(j\omega t)$.

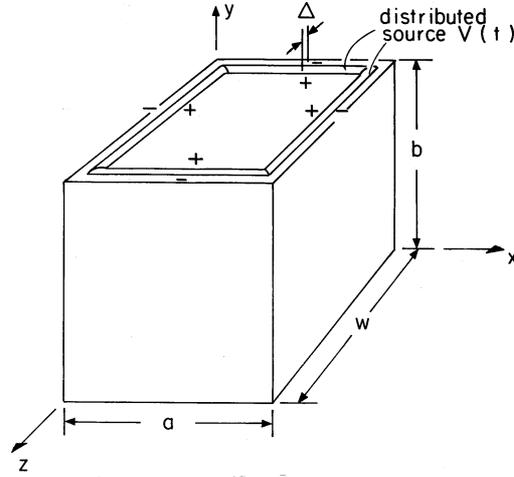(a) Argue that the fields should be TM and use the boundary condition

Fig. P13.4.3

at $y = 0$ to show that

$$\hat{E}_y = \sum_{m=1}^{\infty} \sum_{n=1}^{\infty} 2A_{mn}^{+} \cos \beta_{mn} y \sin \frac{m\pi}{a} x \sin \frac{n\pi}{w} z \qquad (a)$$

[Hint: If (13.4.9) and (13.4.10) are used, remember that $k_y = +\beta_{mn}$ for the A_{mn}^{+} mode but $k_y = -\beta_{mn}$ for the A_{mn}^{-} mode.]

(b) Show that, for m and n both odd, $A_{mn}^{+} = 8\hat{v}(\omega^2 \mu \epsilon - \beta_{mn}^2)/nm\pi^2 \beta_{mn} \sin(k_{mn}b)$, while for either m or n even, $A_{mn}^{+} = 0$.

(c) Show that for these modes the resonance frequencies (normalized to $1/\sqrt{\mu\epsilon}a$) are

$$\omega\sqrt{\mu\epsilon}a = \pi\sqrt{m^2 + \left(\frac{a}{w}n\right)^2 + \left(\frac{a}{b}p\right)^2} \qquad (b)$$

where m, n, and p are integers, m and n odd.

(d) Show that under quasistatic conditions, the field which has been found is consistent with that implied by the EQS potential given by (5.10.10) and (5.10.15).

13.4.4 The rectangular waveguide shown in Fig. P13.4.3 is terminated in a perfectly conducting plate at $y = 0$ that makes contact with the guide walls. However, instead of the excitation electrode shown, at $y = b$ there is the perfectly conducting plate with a square hole cut in its center, shown in Fig. P13.4.4. In this hole, the pole faces of a magnetic circuit are flush with the plate and are used to excite fields within the guide. Approximate the normal fields over the surface of the pole faces as

$$H_y = \begin{cases} \hat{H}_o & \text{for} \quad \frac{a}{2} < x < \frac{a+\Delta}{2} \quad \text{and} \quad \frac{w-\Delta}{2} < z < \frac{w+\Delta}{2} \\ -\hat{H}_o & \text{for} \quad \frac{a-\Delta}{2} < x < \frac{a}{2} \quad \text{and} \quad \frac{w-\Delta}{2} < z < \frac{w+\Delta}{2} \end{cases} \qquad (a)$$
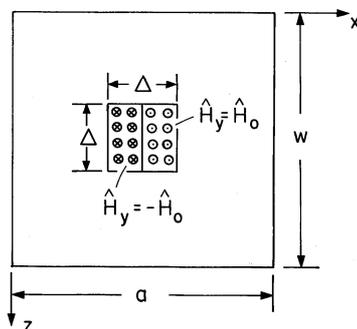
Fig. P13.4.4

where $\hat{H}_o$ is a complex constant. (Note that, if the magnetic circuit is driven by a one turn coil, the terminal voltage $v = j\omega(\Delta^2/2)\mu\hat{H}_o$.) Determine H_y, and hence **E** and **H**, inside the guide.

13.5 Dielectric Waveguides: Optical Fibers

13.5.1[*] For the dielectric slab waveguide of Fig. 13.5.1, consider the TE modes that have E_z an odd function of z.

(a) Show that the dispersion relation between ω and k_y is again found from (13.5.10), but with $(k_x d)$ found by simultaneously solving (13.5.8) and

$$\frac{\alpha_x}{k_x} = -\cot k_x d \qquad (a)$$

(b) Sketch the graphical solution for $k_x d \equiv \gamma_m$ (m odd) and show that the cutoff frequency is again given by (13.5.9), but with m odd rather than even.

(c) Show that these odd modes also have the asymptote of unity slope shown in Fig. 13.5.3.

(d) Sketch the odd mode dispersion relation on that for the even modes (Fig. 13.5.3).

13.5.2 For the dielectric slab waveguide shown in Fig. 13.5.1, $\epsilon_i/\epsilon = 2.5$, $\mu = \mu_o$, and $d = 1$ cm. In Hz, what is the highest frequency that can be used to guide only one TE mode. (Note the result of Prob. 13.5.1.)

13.5.3[*] The dielectric slab waveguide of Fig. 13.5.1 is the same as that considered in this problem except that it now has a permeability μ_i that differs from that outside, where it is μ.

(a) Show that (13.5.7) and (13.5.8), respectively, are replaced by

$$\frac{\alpha_x}{k_x} = \frac{\mu}{\mu_i} \begin{bmatrix} \tan k_x d & ; \text{even} \\ -\cot k_x d & ; \text{odd} \end{bmatrix} \qquad (a)$$

$$\frac{\alpha_x}{k_x} = \sqrt{\frac{\omega^2 \mu_i \epsilon_i d^2}{(k_x d)^2}\left(1 - \frac{\mu \epsilon}{\mu_i \epsilon_i}\right) - 1} \qquad (b)$$

    (b) Show that making $\mu_i > \mu$ lowers the cutoff frequency.
    (c) For a given frequency, does making $\mu_i/\mu > 1$ increase or decrease the wavelength $\lambda \equiv 2\pi/k_y$?

13.5.4 The dielectric slab of Fig. 13.5.1 has permittivity ϵ_i and permeability μ_i, while in the surrounding regions these are ϵ and μ, respectively. Consider the TM modes.

    (a) Determine expressions analogous to (13.5.7), (13.5.8), and (13.5.10) that can be used to determine the dispersion relation $\omega = \omega(k_y)$ for modes that have H_z even and odd functions of x.
    (b) What are the cutoff frequencies?
    (c) For $\mu_i = \mu$ and $\epsilon_i = \epsilon = 2.5$, draw the dispersion plot for the lowest three modes that is analogous to that of Fig. 13.5.3.